Beyond Viscosity Curves: A Critical Rheological Perspectives for Converging Material Extrusion Additive Manufacturing and Powder Injection Molding

Dagmar Endlerova, Martin Novak, Berenika Hausnerova*

[1]Department of Production Engineering, Faculty of Technology, Tomas Bata University in Zlin, Vavreckova 5669, 760 01 Zlin, Czech Republic

*Corresponding author: hausnerova@utb.cz

Abstract: Rheological behaviour of highly filled polymer feedstocks critically governs their processability in material extrusion (MEX) additive manufacturing and powder injection molding (PIM). These converging technologies require robust flow control to achieve defect-free, dimensionally accurate parts. Despite extensive rheology-related literature, clear and transferable links between measured properties and process optimization remain scarce. This review summarizes rheological strategies for improving processing of highly filled compounds, with emphasis on maximum packing, wall slip, yield stress, powder-binder segregation and pressure-dependent flow. It also highlights conceptually inconsistent practices, including the widespread use of simple shear-thinning models for structurally complex feedstocks or activation energy evaluated at a constant shear rate. By focusing on a limited set of physically meaningful rheological parameters and their relation to typical processing failures, the review outlines a framework for material selection and formulation optimization in converging MEX and PIM technologies.

Keywords: Rheology; Material Extrusion; Powder Injection Molding; Viscosity; Wall Slip; Yield Stress

Introduction

The development of materials for advanced processing technologies, such as material extrusion (MEX) additive manufacturing and powder injection molding (PIM), requires a detailed understanding of their rheological properties. These technologies enable the production of complex geometries with high filler content, however, successful processing is limited by severe flow phenomena which still need to be clarified.

Over the past decade, several developments have begun to narrow a traditional boundary between MEX and PIM. Both technologies rely on highly filled powder–binder feedstocks, in principle use similar material systems and debinding as well as sintering cycles, even though their forming steps (printing/injection molding) differ. MEX, in which material is extruded through a nozzle and deposited layer by layer, includes filament-based systems, pellet-based screw-extrusion systems, and slurry-based processes. Filaments must combine sufficient melt flow in the nozzle with solid-state flexibility and toughness for handling, pellet-based screw systems are closest to PIM in terms of high-shear melt deformations, while low-shear stability and yield behaviour is most important for slurries. Recent reviews and case studies on metal and ceramic MEX emphasize that highly loaded filaments and pellets designed as PIM feedstocks can be used to print prototypes, complex internal

channels, e.t.c. [1-5].

MEX and PIM compounds represent a specific class of materials containing significant amounts of inorganic particles - metal and ceramic powders - dispersed in a polymer matrix (binder). Their rheological behavior is influenced by factors such as particle size and shape, surface interactions, filler volume fraction, and the viscoelasticity of the polymer binder. These parameters play a crucial role in optimizing processing conditions and determining the final mechanical and functional properties of the manufactured parts. Flow performance of the compounds is also critical to ensure homogeneous printing/mold filling and minimizing defects such as powder/binder segregation, porosity, or deformations during binder removal. The flow behavior of the material during processing is typically nonlinear and requires precise modeling, which will be even more stringent with rising demand for implementing recycled polymers as binders.

The viscosity of a binder should be less than 0.1 Pa.s to provide highly-filled feedstocks with a viscosity below 10^3 Pa.s [6], but even higher-viscosity feedstocks can be proceeded well at the shear rates relevant for PIM and MEX. The rheological requirements of powder-binder feedstocks depend strongly on the shaping route and must therefore be compared only at a specified deformation mode and shear rate or angular frequency. PIM/MIM feedstocks generally require low apparent viscosity under injection-relevant shear conditions (typically in 10^4 Pa.s) to ensure complete mold filling, whereas filament-based MEX can tolerate higher feedstock viscosities (proceeded typically between 10^2-10^3 s^{-1}) if the filament also provides sufficient feeding stability, strength, and flexibility (Virdhian et al., 2021, Sadaf et al., 2022). Pellet-based MEX avoids the mechanical constraints of filament feeding and can process low-viscosity MIM-like feedstocks when extrusion pressure and strand stability remain controlled (Omrane et al., 2024, Strano et al., 2019). Therefore, feedstock rheological properties should not be compared without specifying whether they refer to oscillatory complex viscosity (rotational rheometer), melt flow rate, melt flow index or “standard” steady shear viscosity obtained with a capillary rheometer at process-relevant nozzle/injection shear conditions (Table 1). The only exception are slurry-based feedstocks, where a steady shear viscosity should be evaluated with a cone and plate rotational rheometer, operating in the low shear rate region 10^{-2} -10^2 s^{-1}).

Table 1 Process-relevant nozzle/injection shear conditions and key flow parameters

Process	**Shear rates**	**Typical viscosity/Key flow parameters**
PIM	$\sim 10^4$ s^{-1}	10^3–10^5 Pa.s; wall-slip, temperature/pressure
Fillament-based MEX	$\sim 10^2$–10^3 s^{-1}	10^2–10^4 Pa.s; elasticity, temperature
Pellet-based MEX	$\sim 10^2$–10^4 s^{-1}	10^3–10^5 Pa.s; wall-slip, temperature/pressure
Slurry-based MEX	$\sim 10^0$–10^2 s^{-1}	exceeds 10^5 Pa.s; yield stress, viscoelasticity

A simple Google Scholar search combining *additive manufacturing* and *rheology* or *powder injection molding* and *rheology* returns well over 17,000 items published in the last decade, yet the field still lacks clear, generally accepted evidence that rheological characterization systematically

leads to robust process optimization. Despite this impressive volume of work, most studies remain highly case-specific: they report detailed flow curves and model fits for a particular powder–binder formulation and part geometry, but rarely translate these data into broadly applicable processing rules or validated design criteria across different systems. In many cases, constitutive models originally developed for far simpler materials are applied to highly filled, separation-prone feedstocks, without addressing key phenomena such as wall slip, pressure sensitivity, yield stress, or segregation in the critical regions of MEX and PIM processes. As a result, rheology is often treated as a mandatory characterization step rather than as a genuinely predictive tool that links measurable material parameters to defect formation, processing windows, and industrial robustness.

This review article is designed to complement previous fundamental works by focusing on the distinct and often under-represented rheological phenomena observed in highly filled MEX/PIM compounds. While former reviews have provided extensive coverage of general rheological characterization methods and results [7], this work aims to specifically address complex behaviors that are increasingly recognized as crucial for practical processing and product quality, Figure 1. These include binder interactions, wall slip, yield stress, segregation effects, instability phenomena, and the influence of pressure.

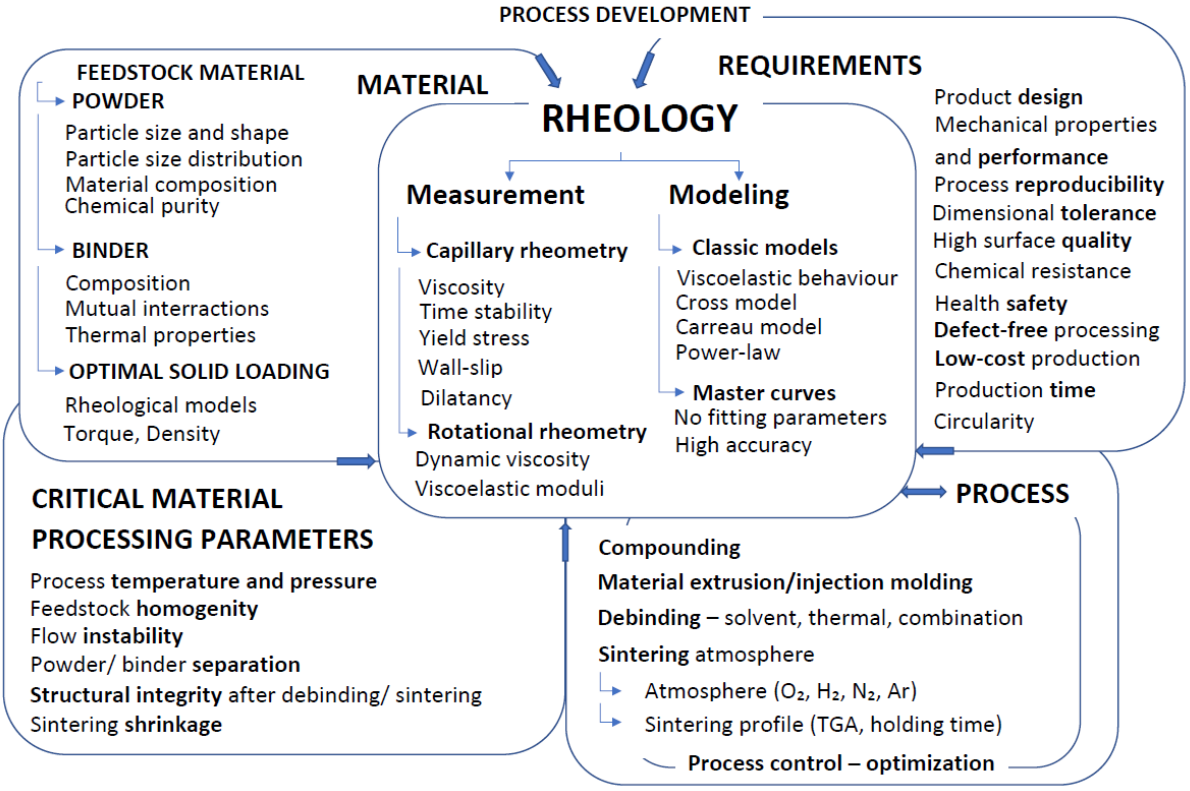

Figure 1 Role of rheology in feedstock design and process development for MEX and PIM.

1. Binder components governing flow performance of feedstocks and their mutual interactions

Successful processing of PIM/MEX compounds requires careful consideration of the rheological

properties of the binders. While significant research has focused on the impact of tailored binder formulations on the rheology of highly loaded feedstocks and the selection of suitable additives, the roles of specific binder components and their mutual interactions remain incompletely understood. Over several decades of development, the principal components of MEX and PIM binders have become relatively standardized, primarily relying on waxes, polyolefins, and polyethylene glycol, Tables 2 and 3. In additive manufacturing, binder compositions are increasingly focused also on liquid organic binders, polylactic acid, and reactive binders as in the early stages of PIM binder developments [8]. Recent works [9-11] examining binder-powder interactions for binder jetting, or reviewing binder development for low-pressure PIM, tend to focus on rheological, thermal (calorimetry and thermogravimetry), or process property relationships rather than directly quantifying the interactions at the molecular level. Most published studies rely on established combinations of well-characterized polymers and evaluate “good” or “poor” performance through viscosity windows, torque response, non-Newtonian (power-law index) or moldability index [12]. Only few go beyond this descriptive level and attempt to separate the effects of individual binder components or to provide transferable design rules. Such an exception is the work by Côté *et* al. [13], which stands out for its comprehensive experimental and numerical analysis of binder constituents and solid loading effects in titanium-based low-pressure powder injection molding. The study formulates and assesses 35 different feedstocks using spherical titanium powder and four binder components: paraffin wax (PW), stearic acid (SA), ethylene-vinyl acetate (EVA), and carnauba wax (CW). By mapping viscosity thresholds, the authors establish the exact proportions needed to optimize moldability, demolding, and segregation prevention. They showed that adding only 0.25 vol.% SA reduced the zero-shear viscosity (at 100 s^{-1}) by a factor of four, whereas further SA addition (up to 5 vol. %) had almost no effect. Increasing EVA content above about 2 vol.% caused a pronounced, almost linear rise in viscosity, while time-dependent tests at a constant shear rate demonstrated that raising EVA from 1 to 2–3 vol.% was sufficient to suppress segregation at high solid loading. In contrast, adding up to 10 vol.% CW changed the reference viscosity by less than about 25 %, but significantly increased thermal sensitivity. Combining flow data with injection molding revealed an optimum binder composition (1% SA, 1% EVA, 3% CW; balance PW) and demonstrated that intricately shaped parts can be molded with up to 64 vol.% solid loading. Their numerical simulations were validated experimentally, providing one of the few examples where binder–composition–rheology relationships are translated into predictive process guidelines rather than remaining case-specific. In the following, the main compositional aspects in binders for PIM/MEX are reviewed and grouped to three main clusters aiming at binder polarity, molecular weight, and interactions, to provide more generally applicable rheological guidance.

Table 2 Overview of binders developed for MEX and PIM

Material	**Processing Method**	**Ref.**

Binder	**Filler**		
CW, PW, PP, LDPE, SA (selected 16PP/22PW/2SA vol.%)	316L (60–66 vol.%)	micro-PIM	[14]
20HDPE/45EVA/25BW/10SA (wt.%)	yttria-stabilized zirconia powder (50 vol.%)	micro-PIM	[15]
50HDPE/46PW/4SA (vol.%)	alumina (58 vol.%	PIM	[16]
PW, PP, PE, SA	niobium powder (57 vol.%)	PIM (molding simulated, no sintering)	[17]
57PW/25PP/15PE/3SA (wt.%)	57zirconia/43mullite vol.% (87 wt.%)	PIM	[18]
60PW/15HDPE/10PP/10PS/5SA (wt.%)	carbonyl iron and carbonyl nickel up to 60 %	PIM	[19]
50PW/50HDPE	17-4PH (66 vol.%)	PIM	[20]
PW, PE, SA and OA	tungsten carbide (42-44 vol. %)	micro-PIM	[21]
79PW/29PE/1SA (vol.%)	SiC (50-56 vol.%)	PIM – no sintering	[22]
85PEG/15PMMA (wt.%)	90stainless steel 304L/10WC (52.5-55 vol.%)	PIM – no sintering	[23]
83-90PEG/10-15PMMA/0-2SA (wt.%)	94WC/6Co wt.% (54-60 vol. %)	PIM	[24]
75-90PEG/10-25PMMA/0-2SA (wt.%)	316L (63-68 vol.%)	PIM	[25]
83PEG/15PMMA/2SA (wt.%)	Inconel 718 (59 vol.%)	PIM	[26]
70-80PEG/20-30PMMA (wt.%) –	316L (65 vol.%)	PIM	[27]
PEG, PVB, SA	alumina (55 vol.%)	PIM – no sintering	[28]
59PEG/12PW/28AW/1SA (wt.%)	316L (60 vol.%)	PIM	[29]
PEG, PE, PW, CW, SA	alumina (84.2 - 86.5 wt.%)	PIM – no sintering	[30]
ABS	iron and copper (up to 50 wt. %)	MEX – no sintering	[31]
74PW/23LDPE/3SA (wt.%)	copper (65 vol.%)	MEX (piston type)	[32]
PW, LDPE, SA	alumina (10-60 vol.%)	MEX	[33]
19-20ABS/7-9PS or PW (wt.%)	iron (70-75 wt.%)	PIM/MEX - no sintering	[34]
57-63ABS/15-19surfactant (vol.%)	copper (22-24 vol.%)	PIM/MEX - no sintering	[35]
60-70nylon/ 6-7.9 plasticizer (wt.%)	iron (30-40 vol.%)	MEX – no sintering	[36]
20wax/19polymer/35tackifier/26 elastomer (wt.%)	Si_3N_4 (up to 55 vol.%)	MEX – no sintering	[37, 38]
44PP/13.9elastomer/18.7 plasticizer/7.8 tackifier/15.6 wax (vol.%)	mullite, fused silica, titanium dioxide (55 vol.%)	MEX	[39-41]
polyolefins, hydrocarbon resin, SA	lead zirconate titanate and hydroxyapatite up to 55 vol.%	MEX	[42, 43]
TPE, polyolefin, dispersants	316L, Ti_6Al_4V, NdFeB, $SrFe_{12}O_{19}$, zirconia	MEX	[44-50]
PA, PLA, stearates	316L (up to 55 vol. %)	MEX	[51]
60-70 polyamide 12 (wt.%)	zirconia/(βTCP)	MEX – no sintering	[52]
27.5SEBS/27.5PW/10SA/HDPE (vol.%)	zirconia (47 vol.%)	MEX	[53]
PEG	stainless steel (79 vol.%) and zirconia (84.2 vol.%)	MEX (screw type)	[54]

Table 3 Examples of MEX/PIM patent claims

surfactants, mold release agents, polyacetal, plasticizers (0.5-2/0.05-1/15-50/1-10 wt.%), other materials (LDPE, aPP, EVA, waxes and their mixtures); total 15-50 wt.%	ceramic powders such as alumina, zirconium, silicon dioxide, silicon nitride, silicon carbide (50-85 wt.%)	[55]
polyoxymethylene mix (35-60 vol.%), dispersants (0-5 vol.%)	sinterable inorganic non-metallic powder (40-65 vol.%)	[56]
agar (1.5-10 % wt.%), additives (sugar, gel strengthening agents, acids, bases, biocides, sodium silicate, borate,	copper (50-97 wt.%)	[57]

antioxidants, lubricants, dispersants, plasticizers, compatibilizers, surfactants), and water (5-11 wt.%)		
three-component binders: PEG or polypropylene glycol or PVA, PS or dioctyl phthalate, and a strengthening component (PE)	ceramics, metals, and cermets powder/binder ratio: 7/3 or higher	[58]
38-67 wt.% partially hydrolyzed PVA, 8-32 wt.% PP or PE, and 25-35 wt.% processing aids (3-19 wt.% water, and 9-19 wt.% plasticizer (glycerin)	at least 70 wt.% of a powdered metal or ceramic	[59]
hydroxybenzoic acid-behenylester, 4 hydroxybenzoic acid-ethyhexylester, PA6, PA12, SA	ceramic or metal powder (80-95 wt.%)	[60]
HDPE, isopropyl tri(dioctyl)pyrophosphato titanate, tri(dioctyl)phosphato zirconate, surfactants	metal or ceramic powder (30-99 wt.%)	[61]
50-96 polyoxymethylene/2-35polyolefin/2-40 others (polyether, polyurethane, epoxide, polyamide	inorganic powder (40-70 vol.%)	[62]

1.1. Polarity and powder-binder adhesion

Polarity of binder to powder is the first attempt to suitable rheological performance and successful PIM/MEX processing. Most often used binder components as polyolefins and paraffin wax are essentially non-polar, thus their adhesion to highly polar powders requires further compositional wettability treatment. Zaky *et* al. [63] investigated the influence of paraffin wax (PW) characteristics on the rheological behavior of 17-4PH stainless steel feedstocks. They evaluated various types of PW in combination with a poly(ethylene-co-vinyl acetate) (EVA) copolymer and compared their performance in compression and injection molding. The selected wax with the highest molecular weight, crystallinity and branching index revealed viscosity of 56 vol. % feedstock well below 10^3 Pa.s at 10^4 s^{-1}. Block copolymers as EVA have been identified as effective steric stabilizers improving feedstock homogeneity and stability upon shearing much earlier [64] - one block of the polymer is soluble in the binder, while the insoluble block adsorbs onto the powder surface, thus serving as an anchor between the powder particles and the binder. The importance of block copolymer type (EVA, EBA - ethylene-butyl acrylate, or EAA - ethylene-acrylic acid) was found to decrease with powder loadings from about 67 % for the pure binders to only 10 % for feedstocks above 30 vol.% [64], however, EVA is still most preferred copolymer in PIM applications. Considering MEX, Marnot *et* al. [65] also discusses the use of block copolymers in the recent review, where EVA copolymer has been highlighted for its effectiveness in improving the dispersion of metal powders in polymer matrices, thereby enhancing the printability of highly loaded feedstocks.

Similarly, several studies on wax and surfactant selection have highlighted that seemingly small changes in binder formulation can dramatically alter flow behaviour and segregation tendency. Karatas *et* al. [66] investigated the influence of various waxes (carnauba wax, beeswax, and paraffin wax) combined with a polyethylene-based binder on the rheological behavior of 50 vol.% steatite feedstocks and showed that the substitution of 55 wt.% paraffin wax and 10 wt.% stearic acid with 50 wt.% carnauba wax resulted in 50 % decay of feedstock viscosity at 100 s^{-1}. However, it is important to note that the carnauba wax-based feedstock was prepared without stearic acid, thus it remains unclear whether the superior performance can be attributed to the presence of paraffin wax or stearic

acid additive.

Muranov *et* al. [67] compared the rheological behavior of 61.9 vol% 42CrMo4 steel powder feedstocks formulated with a two-component paraffin wax–polypropylene binder system against those prepared with a polyoxymethylene (POM) binder. Their study highlighted that wax–polyolefin binders exhibited significantly lower viscosity, which is advantageous for molding thin-walled products; however, they also showed higher sensitivity to shear rate gradients (power-law exponent *n* of 0.26–0.36 compared 0.47 for the POM feedstock) leading to issues such as jetting and component segregation during molding. In practical terms, a suitable feedstock for PIM/MEX should combine viscosity in the target processing window with a moderate power-law index.

It should be also stressed that low polarity of some waxes often results in segregation of powder and binder even during low-pressure powder injection molding as addressed by Fareh *et* al. [68]. They investigated the impacts of testing time, shear rate, polymer degradation, powder deagglomeration, and temperature on the rheological properties of wax-based feedstocks. Importantly, they showed that for low-viscosity systems (40PW and 35PW+5SA), the long tests caused a flow change from pseudoplastic behaviour to a dilatant regime (with viscosity increase of nearly 40 %). Their findings concluded that viscosity profiles must be obtained over short rheological test durations to minimize the risk of segregation. The cause of segregation, however, is not always easily detectable in multicomponent binders as demonstrated for carbide feedstocks containing only two components - paraffin wax (PW) binder and polyethylene glycol-based (PEG) binder [69]. In the PW-based system, capillary flow was blocked at shear rates around 1000 s^{-1} due to segregated PW, whereas the PEG-based feedstock exhibited only a distinctive jump (in an order of magnitude) in viscosity at this critical shear rate. There the segregation manifested as a blockage of a capillary was clearly a consequence of poor adhesion and insufficient wetting of nonpolar paraffin wax toward the carbide powder, while the PEG-based feedstock retained flow because of the better PEG binder affinity to carbide powders.

Abdullah *et* al. [70] investigated the influence of palm stearin wax content in a low-density polyethylene (PE-LD) binder on the rheological behavior of Inconel 718 feedstocks. They found that increasing the wax content up to 70 wt% resulted in a significant reduction in viscosity and flow activation energy, thereby enhancing the moldability of the feedstock. Park *et* al. [71] utilized three different binder formulations, each comprising a backbone polymer (polypropylene or polyethylene), main body (paraffin wax, carnauba wax, microcrystalline wax) combined with stearic acid as an additive. The findings revealed that feedstock with the highest portion of waxes (60 wt%) and powder loading of 45 vol.% exhibited optimal flowability (viscosity reduced by a factor 2-3 in the shear rate range from 10^2 to 10^3 s^{-1}), emphasizing the significance of selecting an appropriate binder composition to achieve desirable rheological properties.

Importantly, Forstner *et* al. [72] emphasised that binder optimization for MEX cannot target low viscosity, but must balance it with sufficient ductility. On 60 vol% metal powder (1.2343 tool steel) feedstocks with binders composed of PE, PP and hybrid PE/PA waxes combined with PE-LD, they

showed that PE- and PP-based feedstocks were successfully printed using MEX at rather high temperatures (200°C and 240°C), whereas the third feedstock containing PE/PA wax was too brittle for an effective processing, leading to filament breakage before extrusion; regardless of a substantial (more than 90 %) decay in viscosity (melt volume rate increased from about 5 cm^3/10 min for the wax-free reference to 130 cm^3/10 min) they reduced the elongation at break to around 0.3 % and raised the minimum bending radius well above the 60 mm threshold required for spooling.

Urtekin *et* al. [73] applied Taguchi orthogonal arrays to minimize the number of experiments while capturing main effects and interactions for stainless steel powder filled with three different binder systems (PW/CW/SA, PW/PE/SA, and PEG/PP/SA). ANOVA analysis was used to quantify the contribution of temperature and powder loading to viscosity, and to build empirical equations relating these responses to the control factors. The results show that both temperature and solid loading strongly affect flow, but their relative influence depends on the binder system.

Overall, the work of Hsu *et* al. [74] from 1994 still offers the most valuable insight into the effects of different wax compositions on the injection molding of carbonyl iron powder with PE-LD. The researchers compared paraffin wax, polyethylene wax, carnauba wax, and acrawax, finding that polar waxes like carnauba and acrawax exhibited stronger interactions with iron powder, leading to higher viscosity and better pseudoplasticity. The study highlights the importance of wax selection in achieving desired rheological properties and final part quality.

Sufficient wettability of mon-polar waxes and polyolefin binders is usually attained with processing additives (surfactants). Tseng [75] explored the effect of three different surfactants - stearic acid (SA), oleic acid (OA) and 12-hydroxystearic acid (HSA) on rheological properties of the 60 vol% alumina compounds and resulted in the viscosity order $\eta_{SA}<\eta_{OA}<\eta_{HSA}$ (1500, 3000 and 5000 Pa.s, respectively) showing the strong dependency of the agglomerates formation with the HSA suspension exhibiting the highest initial yield stress ($\tau_{y,HSA}>\tau_{y,OA}>\tau_{y,SA}$) and a temperature-induced drop by more than 300 kPa between 120 and 150 °C, showing that surfactant choice strongly governs agglomerate strength and network breakdown confirmed with the yield elimination and turning the flow to a pseudoplastic manner after repeated shearing. Recently, researchers examined the effects of different binder systems on the rheological and magnetic properties of Nd-Fe-B feedstocks intended for PIM. The study evaluated binder formulations with varying ratios of linear low-density polyethylene (PE-LLD), paraffin wax (PW), and SA. It was observed that a binder system containing 35 vol.% PE-LLD, 60 vol.% PW, and 5 vol.% SA provided optimal flow behavior - viscosity decreased from about 750 Pa.s to 300 Pa.s at a shear rate of 100 s^{-1}, and from 330 Pa.s to 130 Pa.s at 1000 s^{-1} compared with a more PE-LLD backbone-rich and less-additive binder (52.5 vol.% PE-LLD, 41.25 vol.% PW, and 6.25 vol.% SA), while maintaining stable pressure traces with only ~0.4% fluctuation, indicating good homogeneity. and minimized contamination. This composition led to improved density and magnetic properties in the sintered parts, highlighting the critical role of surfactants in achieving desirable feedstock characteristics [76].

1.2 Molecular weight of binder components

Generally, lower molecular weight binder components fulfill the primary role of a binder to facilitate easy mold filling or extrusion via reduction of zero-shear viscosity as well as non-Newtonian index (viscosity is more sensitive to shear rate). However, both research and practice show the opposite requirement - increasing molecular weight is often desirable to balance still suitable viscosity with shape retention and flow stability against segregation upon high shearing and temperatures.

Water-soluble polyethylene glycol (PEG) is most often utilized binder component, whose molecular weight is varied and tailored to particular powder features and feedstock composition. Eickhoff *et* al. [77] investigated the effects of PEG with molecular weights ranging from 2000 to 20 000 g/mol on the compounding behavior of 60 vol% Ti6Al4V feedstocks for additive manufacturing. They combined PEG with either PVB (poly(vinyl butyral)) or PMMA (poly(methyl methacrylate)) and observed that higher molecular weight PEGs can enhance the viscosity of the feedstock, which was crucial for achieving optimal flow behavior during the printing process. At a shear rate of 10^3 s^{-1}, the apparent viscosity of PEG/PVB increased (from less than 10^2 Pa.s for PEG 2000 up to 200 Pa.s for PEG 20 000). For PEG/PMMA feedstocks the viscosities were about one decade higher than for PEG/PVB at the same solid loading (due to much higher PMMA molecular weight of ~159 000 g/mol), and the variation of PEG molecular weight between 2000 and 8000 g/mol had only a minor effect on viscosity level of PEG/PVB, although all compositions still showed shear-thinning suitable for filament extrusion.

Elbadawi [78] examined how varying molecular weights of PEG influence polycaprolactone (PCL) MEX filaments loaded with ciprofloxacin. The study revealed that lower molecular weight PEG (e.g., PEG 200 g/mol) significantly reduced complex viscosity; in the range from 10^{-2} to 10^2 s^{-1} PCL viscosity dropped down about one order of magnitude for PCL/PEG 200 (from 10^4 Pa.s to 10^3 Pa.s), enhancing flow but potentially compromising structural integrity. In contrast, higher molecular weight PEG (e.g., PEG 8000 g/mol) increased PCL viscosity (PCL/PEG 8000 was about 1.5–2.5times higher), but improved shear-thinning behavior, solidification rates, and adhesion strength, making it more suitable for printing applications.

These findings correspond to earlier works devoted to PIM. The findings on titanium [79], Inconel 718 [26], or alumina [80] PIM feedstocks indicate that feedstocks with higher molecular weight PEG exhibit increased viscosity and yield stress resulting in reduced flowability. On the other hand, lower molecular weight PEGs (1000 and 1500 g/mol) enhance fluidity but lead to shear thickening (non-Newtonian index from 1 to 1.5 in temperature range 70 – 110 °C) attributed to binder-powder separation at elevated temperatures [80]. The viscosity of 55 vol% alumina feedstocks with PEG1000 and PEG1500 was less than 20 Pa.s at a shear rate of 200 s^{-1}, whereas increasing PEG molecular weight to 20000 g/mol raised the viscosity to 80–100 Pa.s, but in shear thinning manner with non-Newtonian index ranging from 0.7 to 0.5 in the temperature range 80 -130 °C.

Regardless of a strong effect of molecular weight on viscosity and flow stability, other binder components than PEG have been hardly investigated. One of very rare exceptions is work by Gonzalez-Gutierrez et al. [81] studying a possibility of lowering viscosity of POM, a backbone binder used in commercial PIM and MEX feedstocks by BASF, which provides excellent mechanical strength to the manufactured parts, but has high viscosity, which complicates processing. On a set POMs with molecular weights ranging from 10 000 g/mol to about 130 000 g/mol, it was observed that POM viscosity increases with molecular weight at a faster rate than impact toughness - reduction of molecular weight to 24 000 g/mol decreased POM complex viscosity by three orders of magnitude (from 10^3 Pa.s to 1 Pa.s), while maintaining comparable mechanical performance.

1.3 Molecular-level interactions among binder components

The interactions among binder components are, in the vast majority of cases, deduced from their rheological performance. More direct evaluation is a challenging task due to the significantly strong self-interactions of polymers. Chen and Wolcott [82] employed differential scanning calorimetry and atomic force microscopy to evaluate the morphology and crystallization of nonpolar paraffin (PW) and polyethylenes (PE-HD, PE-LD, and PE-LLD). The obtained data served as an evidence of a partial miscibility of PW in polyethylenes with PE-LLD/PW being favorable over the PW/PE-HD. Sudhakar and Selvakumar [83] reported on the miscibility of chitosan and PEG blend using a buffer solution. From collected FTIR spectra for polyblend films and polymers, it was observed that with increasing the amount of PEG, the O–H stretch peak tends to lower peak wavenumbers, serving as the evidence of the component's miscibility. Doulabi *et* al. [84] quantified the interaction parameters of PEG and chitosan by using viscosity, density, and refractive index evaluations. The results showed that the components at 80 % or higher chitosan concentration were miscible by means of intermolecular hydrogen-bonding interaction between hydroxyl groups of polyethylene glycol fumarate with amino and hydroxyl groups of chitosan.

Ucar *et* al. [85] studied surface properties of EVA, PE-HD and polyvinyl acetate PVA blends using contact angle analysis and X-ray photoelectron spectroscopy. Tested EVA samples varied in the content of vinyl acetate in the range from 12 to 33 wt.%. Thin layers of each blend were prepared from their xylene solutions at high temperatures by a dip coating technique. Static and dynamic contact angle measurements were carried out using grade water, methylene iodide, ethylene glycol and formamide. The obtained data showed that the increase of the polar hydrophilic vinyl acetate in the blend resulted in the decrease of the water equilibrium contact angles, thus enhancing wettability.

The surface energies of low-density polyethylene (PE-LD), polyethylene glycol (PEG), paraffin wax (PW), carnauba wax (CW), acrawax (AW) and stearic acid (SA) components of Al_2O_3 and ZrO_2 feedstocks were determined from the measurements of contact angles of three testing liquids (deionized water, ethylene glycol and diiodomethane) [86]. Low contact angles measured for PEG in all testing liquids could be explained by the hydrophilicity of its surface. Contact angles for CW and

SA exhibited very similar values in water, and crosswise for the remaining testing liquids. In this view, it seems that CW could overtake the role of a plasticizer in binders. Interestingly, AW exhibited the values of contact angle comparable with those obtained for PW, where no adhesion is expected.

Recent studies of MEX also address binder-powder and binder-binder interactions, but generally focus on process parameters and macroscopic outcomes such as print fidelity, residual binder analysis, and defect formation. There are reports of calorimetric and FTIR measurements in these fields, especially for studying binder decomposition and powder compatibility [87], but true molecular-level, quantification remains extremely rare.

One option to quantify interactions is to employ low molecular weight analogues of binder polymers, which simplify the system and allow precise FTIR and calorimetric analysis of feedstocks [88], [89]. In the model systems, self-interactions of long polymer chains are largely eliminated, so that the interactions between individual binder components become visible. The results show that the binder components such as PEG, CW or AW, which may have very similar effect on feedstocks viscosity values, can exhibit markedly different interaction energies and miscibility, which then manifest as differences in flow causes (thinning/thickening) and segregation tendency. Through calorimetric measurements of the analogues, the studies quantify the energies of mutual associations in various combinations, while FTIR analysis tracks characteristic spectral shifts as evidence of molecular interactions such as hydrogen bonding. For CW/PEG system, the findings demonstrate partial miscibility and beneficial interactions, while AW/PEG analogues exhibit approximately twice as strong interactions (hydrogen bonding between CO and NH groups) leading to more favorable processing characteristics for MEX/PIM applications. By providing quantitative guidelines and highlighting the compatibility of particular binder combinations, these studies advance the rational design of binder systems for improved rheological behavior and process stability.

Chapter summary:

- Binder composition remains the most powerful, yet least systematically explored, approach to defect-free manufacturing of MEX/PIM parts. Most binder studies establish “good” viscosity windows for specific powder–binder systems, but only few derive generally transferable and applicable rules. Quantitative interaction studies are rare, even though they offer a route to data-driven binder design beyond trial and error.
- Although lower molecular weight binder components fulfill the primary role of a binder to facilitate easy mold filling or extrusion, they may lead to shear thickening attributed to binder-powder separation. Thus, the increasing molecular weight is often desirable to balance still suitable viscosity with shape retention and flow stability.
- Low polarity of polyolefins and some waxes result in a powder-binder segregation due to poor adhesion and insufficient wetting of highly polar powders. Except of surfactants (stearic acid), block copolymers are particularly effective in improving dispersion of powders in binders, thereby enhancing their printability and moldability – even additions as low as for surfactants (1-3 wt%)

suppress powder-binder segregation.

- Suitable feedstock for PIM/MEX should combine viscosity in the target processing window with a moderate (~0.5) power-law index. For MEX it must also balance it with sufficient ductility.
- Practice-relevant advice: For new formulations, start from a proven backbone (polyolefin + wax) with a modest amount of polar component or surfactant, to balance three competing requirements: moderate viscosity for filling, low tendency to powder/binder segregation, and debinding without a part distortion.

2. Rheological approaches essential for determination of powder loading

A capillary rheometry remains the most widely used tool to determine the relative viscosity of MEX and PIM feedstocks necessary to calculate the maximum packing fraction for a given composition. However, torque rheometry and simple mixing-torque measurements often provide a more direct and practically relevant route to identify the processable powder loading, especially during early formulation screening.

As powder concentration approaches the maximum packing fraction, binder is entirely squeezed into the gaps between particles, quickly growing relative viscosity signaling the upper processable limit. The optimal powder loading in the feedstock is then defined as the concentration of powder, where the compound maintains still favorable flow characteristics, along with homogeneity and stability throughout a shear rate window between 10^2 and 10^5 s^{-1}. Dihoru *et* al. [90] showed that this optimum is often 6–14% below the maximum packing, based on torque measurements and neural-network analysis of feedstocks with bimodal powder mixtures. The upper loading limit is dependent on powder features and how packing is arranged. An ideal PIM powder, according to German and Bose [8], incorporates a rather broad size distribution with spherical or nearly spherical particles, enhancing packing efficiency. Combining multiple particle size fractions in powder-binder feedstocks for MEX and PIM enables higher solid loading [20, 91-96].

In practice, some PIM researchers combine torque rheometry with capillary rheology. Torque curves recorded during stepwise powder addition typically exhibit three regimes: a low-sensitivity region at low loadings, a gradual increase in torque as particle–particle interactions become relevant, and a sharp rise beyond a so-called switch point (SP) or critical solids loading (CSL) [14, 97], Figure 2. The CSL indicates the onset of poor wetting and insufficient binder coverage, whereas the SP can be used as a practical measure of the upper recommended loading for stable flow.

For MEX feedstocks, similar strategies are being adopted: optimal powder loading is determined from mixing torque or extrusion-pressure curves, and then related to the filament's extrudability and printability. Several MEX studies report that attempting to push the powder content too close to the theoretical maximum packing leads to brittle filaments, excessive die pressure or severe surface defects, even when the apparent viscosity at moderate shear rates remains within an acceptable range.

This again underlines that critical solids loading is a structural limit rather than a purely rheological one, and that torque-based methods remain valuable screening tools for both MEX and PIM.

According to German and Bose [8], more than one hundred empirical and theoretical expressions have been proposed to derive the maximum packing fraction. Abu-Lebdeh *et* al. [98] explored how well empirical particle packing models can predict the maximum packing density of boron powders for additive manufacturing. The researchers performed controlled experiments with two sets of boron powders having different particle sizes and then mixed them in various ratios to determine their packing densities. They applied both the Furnas ternary model and a modified Toufar binary model to these systems. Their results showed that both models closely matched the experimental data.

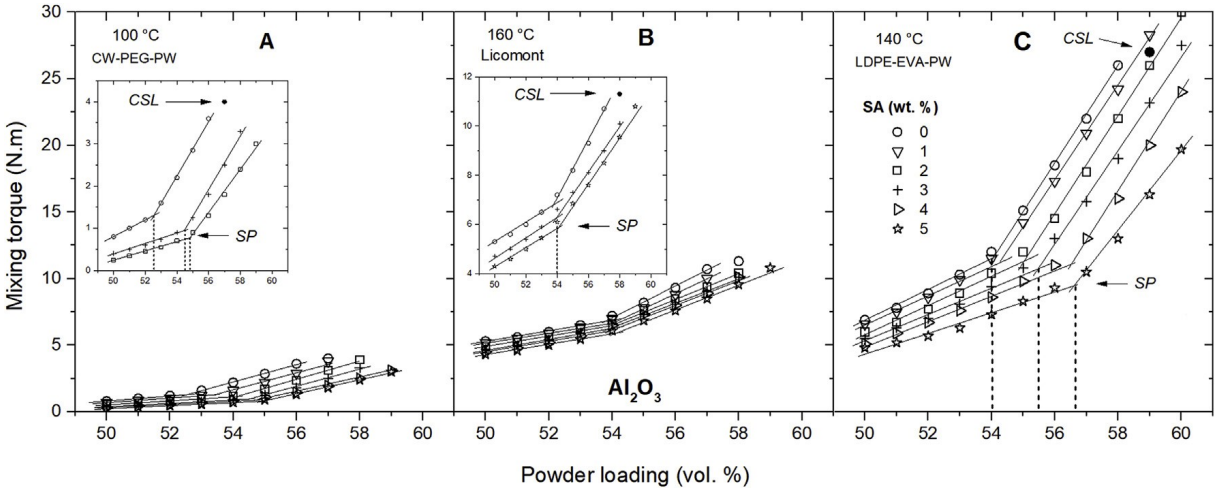

Figure 2 Evaluation of critical solid loading (CSL) and switch point (SP) from torque dependence on Al_2O_3 powder loading in feedstocks differing in binder composition (with permission from [97]).

Nevertheless, there is no single “universal” viscosity model available for highly filled feedstocks. For any given powder–binder system, several models can usually be fitted to the experimental flow curves with comparable quality, especially when particle shape and polydispersity are included as fitting parameters. However, different models fitted to the same data often predict noticeably different values of the maximum packing fraction: Honek *et* al. [99] systematically compared more than fifteen relative viscosity models for hard-metal carbide feedstocks and found that the resulting maximum packing can differ by several volume percent, even when all models reproduce the measured viscosity within the experimental scatter. From a processing viewpoint, such differences are far from negligible, as they may translate into a shift from a robust processing window to a feedstock that exhibits edge cracking, jetting or powder–binder separation.

More physically based approaches, such as hard-sphere (HSM) or virtual-packing models, offer an attractive alternative. In these models, the input parameters are only powder size distribution and loading to reconstruct a virtual 3D particle structure, from which structural descriptors as nearest-neighbor distance distributions, binder-channel width distributions and histograms of groups of close particles (GCP) can be derived and quantitatively correlated with viscosity data [100, 101].

For a set of extruded carbide compounds, HSM model showed that at a fixed solid loading and binder composition, variations in the particle size distribution considerably affects viscosity values and its overall cause – fine (D_{50} 1.36 μm), more agglomeration-prone powders with higher GCP lead to high viscosities (10^5 Pa.s at 10^2 s^{-1}) and apparent yield behaviour at powder loadings above 30 vol.% [100], while coarser powders (D_{50} from 5.28 μm to 15.38 μm) provide significantly lower viscosity (10^3 Pa.s at 10^2 s^{-1}) even at 50 vol.% loading. These models confirm that the influence of powder morphology integrated as an input parameter (particle size distribution in HSM) can be quantified as their output (GCP in HSM) and directly connected to feedstock rheological performance. The advantage is that the model parameters reflect easily measurable powder characteristics rather than introduce empirical fitting constants with no physical meaning. Nevertheless, such models are still rarely used in MEX/PIM development, and their predictions are only occasionally validated against real processing defects.

Chapter summary:

- There is no universally valid viscosity–powder loading model for highly filled systems used in MEX/PIM; different relative viscosity relations can fit the same data yet predict significantly different maximum/critical packing values, so their application should be used with an extreme caution.
- Torque-based methods offer an experimentally simple way to identify the critical powder loading. An optimum processability is associated with a steep but stable increase of torque with increasing powder loading regardless its particular value. An early unstable torque development upon adding powder, which does not stabilize with time, should be considered as a sign of any or very narrow processing window. The combination of torque and capillary flow measurements provide reliable base to define processing windows.
- Feedstock structure based (physical) models which explicitly reconstruct powder packing (hard-sphere and virtual-packing approaches) can link powder characteristics (size distribution, shape, solids loading) to viscosity without overfitting, but they are still rarely used as standard design tools in MEX and PIM.

3. Constitutive models, processing parameters, and their limitations in MEX/PIM

Direct and systematic investigation of the link between rheological characteristics and processability of feedstocks is rare in the literature. Most studies still focus on fitting constitutive relations to viscosity data, rather than demonstrating how these parameters improve the prediction of defects or processing windows. The most commonly used rheological model for describing PIM- and MEX-based feedstocks is a power-law (Ostwald–de Waele) model, which captures their steady non-Newtonian region only. The Carreau and/or Cross models intercepting also the zero-shear plateau and

transition regions are integrated into the simulation tools. Detailed description of the relevant models (Figure 3) can be found in [102].

However, as shown e.g. by Kukla *et* al. [103], any of the fundamental models is not able to capture typical rheological phenomena of highly filled systems such as yield stress and wall slip (Figure 4). In other words, they reproduce the measured shear-viscosity curves but ignore key features that strongly affect flow in thin sections, near walls and in regions prone to segregation.

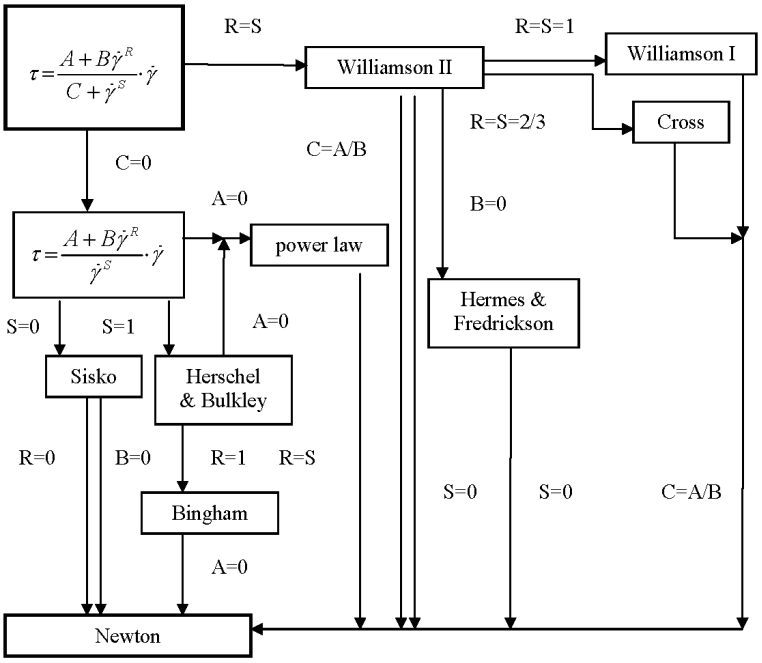

Figure 3 Overview of relevant basic rheological models for MEX and PIM feedstocks (with the permission from [102]).

Empirical models for predicting viscosity as a function of polymer binder formulations were proposed by Gonzalez-Gutierrez *et* al. [104]. Also, Khakbiz *et* al. [105] conducted experiments with capillary rheometry to reveal how parameters as solid fraction, shear rate, and temperature affect feedstock stability for injection molding, proposing an "instability index" but not extending the study to actual molding trials. Suri *et* al. [106] instead used a torque rheometer to examine flow stability, assessing its evolution over time and noting that improved homogeneity in mixing positively affected rheological behavior, yet, once again, no direct quantitative correlation to process performance was made. Zauner *et* al. [107] highlighted that variability in viscosity is related to the dimensional

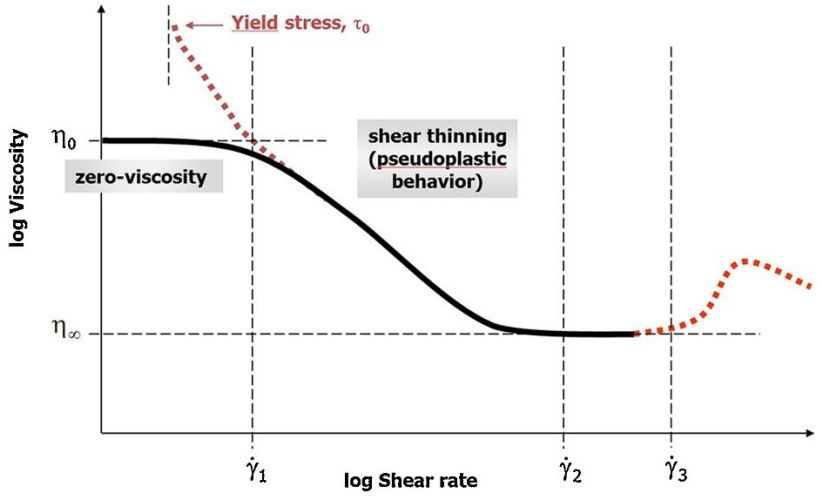

Figure 4 Typical flow curve of highly filled compounds exhibiting yield stress and dilatancy (red-dotted) compared to typical flow curve of polymer melts (with the permission from [103]).

consistency of powder-injected molded products. Meanwhile, Pettas *et* al. [108] showed that during MEX, greater shear rates and longer relaxation times lead to increased dimensional instability of extruded filaments; here, process stability can be described via pressure or viscosity stability, or via consistency of filament diameter as it exits the die, which is also influenced by die swell and gravity.Thus, although it is well accepted that lower viscosity typically enhances processability, robust experimental studies mapping this relationship for highly loaded, extrusion or injection-molded compounds remain uncommon. Taken together, these studies confirm that viscosity is important for process stability, but they rarely provide transferable criteria such as critical viscosity windows or instability thresholds applicable across different materials and geometries.

Against this background, the validation and advancement of the master-curves approach for modelling rheological behaviour offer a promising alternative toward more general, formulation-based descriptions of viscosity [109-111]. The approach was introduced by Filip *et* al. [109] and builds on a capillary rheometry data obtained at processing-relevant shear rates (100–1000 s^{-1}). In practice, the master curve is constructed by measuring shear viscosity for a varied set of feedstock compositions – in this work comprising 36 combinations of 0–50 vol% Al_2O_3 powder loading and 0–5 wt% stearic acid concentration. The measured viscosity data are then expressed through a single algebraic relation: $\log(\eta) = B1(SA\,\%, filling\,\%) + [B2(filling\,\%)] * [3 - \log(\dot{\gamma})]$, where parameter $B1$ depends on both powder loading and SA content, and $B2$ depends only on powder loading. For a new composition within the validated range, viscosity at any shear rate is obtained simply by inserting the known powder and SA concentrations into explicit analytical expressions for $B1$ and $B2$.

Unlike classical models that require several empirical parameters for each feedstock modification, the master curve approach allows for accurate and quick prediction of viscosity using only component concentrations and shear rate. The flow behavior can thus be reliably mapped for a broad range of powder loadings and additive levels, which is key for practical mold design and feedstock optimization, Figure 5. The deviation from experimental values is no greater than typical measurement

error (for shear viscosity measurement approx. 5 %), showing this method's efficiency and utility for industrial applications; it can be used to quickly and reliably anticipate the effects of formulation changes on viscosity.

This approach eliminates the currently used non-Newtonian (power-law) index, by means of which the logarithmic derivative was approximated. The application of master curves is straightforward and does not involves any adjustable parameters. It provides smooth continuous passages among various inputs, and cover not only the measured values but also of all intermediate combinations. As such, this method moves beyond descriptive rheology - it offers a quantitative, transferable tool for efficiently optimizing processing windows and stability in injection molding applications.

Rheological characterization of MEX/PIM feedstocks must also consider the influence of processing conditions - temperature and pressure. Temperature sensitivity is commonly described via the activation energy of shear flow (see Supplementary Material Table S1 for an overview). While German [6] proposed increasing activation energy with higher powder loading, arguing that in filled systems the apparent viscosity drops more rapidly with temperature because the effective volume fraction of solids changes due to different thermal expansion of powder and binder, Shenoy [112] suggested the opposite trend, since rigid particles do not contribute to free-volume changes, making the composite less temperature-sensitive than the neat binder.

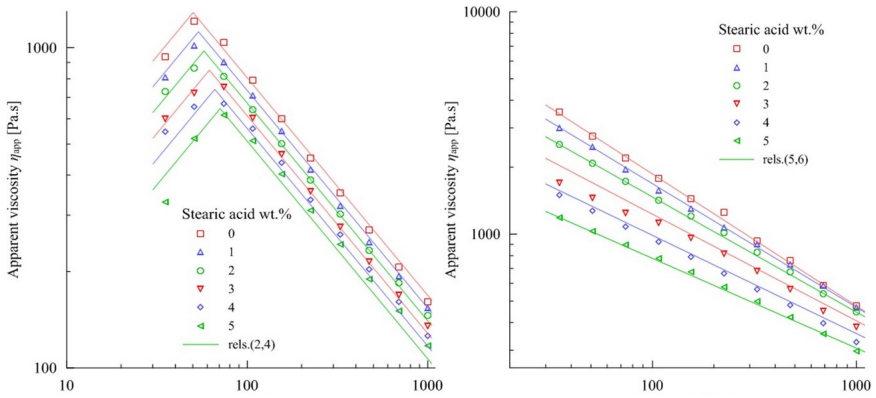

Figure 5 Approximation of apparent viscosity of dilatant/pseudoplastic (Licomont commercial binder) and pseudoplastic (CW/PW/PEG binder) Al_2O_3 feedstocks with master curves (with the permission from [97]).

Recent studies report that activation energy decreases as powder loading increases up to the optimum filling. As an example, Naranjo *et* al. [113] discusses limits for material suitability in terms of shear stress and activation energy providing activation energy values for several volume fractions of 17-4PH hybrid feedstocks for MIM and MEX. Activation energy is evaluated at fixed shear rates representative of PIM (1000 s^{-1}) and MEX (100 s^{-1}). The trend reported is that activation energy

decreases with increasing powder content in the processable range, i.e., higher loading makes viscosity less temperature-sensitive, Figure 6.

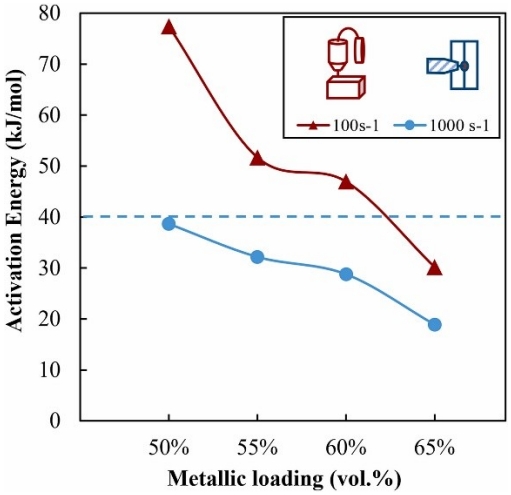

Figure 6 Activation energy as a function of powder loading for typical MEX and PIM shear rates (with permission from [113]).

Further, recent works [114-116] on Ti-6Al-4V and zirconia feedstocks evaluate activation energy from Arrhenius fits at fixed shear rates for several loadings, mainly to define an optimal feedstock window. Their qualitative conclusion is again that activationenergy drops as solid loading increases up to the optimum, i.e., highly filled but still processable compounds are less temperature-sensitive than the neat binder. Interestingly, Contreras *et* al. [117] found - for a comprehensive set of three bronze and four Inconel 718 powders - that activation energy decreases with powder content only up to the optimum loading of a given feedstock, and then increases again once this optimum is exceeded. This behaviour suggests that activation energy can serve as a practical indicator for identifying the optimum powder loading: a decrease with loading followed by an increase may signal that the system has reached the critical loading level. Honek *et* al. [118] reported that activation energies evaluated in the relatively broad temperature range (from 140 to 200 °C) followed Arrhenius relation only in the stable flow regime (without pressure oscillations) for carbide feedstocks; once flow instabilities appear, the concept of an Arhenius activation energy fails, which again underlines that activation energy can be interpreted as a flow stability parameter.

At this point, it should be noted that the vast majority of authors evaluate activation energy at a fixed shear rate. Dimitri *et* al. [119] correlated activation energy for 17-4PH feedstocks with particle size, moldability index and solids loading based on activation energy evaluated at fixed shear rate values. Ahmad *et* al. [115] evaluated Ti–6Al–4V MIM feedstocks; viscosity was measured in a capillary rheometer at several temperatures and defined shear rates, and activation energy was extrapolated from Arrhenius plots at those shear conditions. Amin *et* al. [114] reported flow activation energies for several zirconia loadings again using capillary data at a fixed shear rate. The review by Momeni *et* al. [11] summarizes multiple micro/nano-feedstock studies where Arrhenius linear trend

was derived also at a constant shear rate. Recent MEX feedstock developments with tool steel and bio-based binders also treat temperature dependence via Arrhenius fits of viscosity at selected shear rates relevant for extrusion, although many papers focus more on printable temperature windows than on explicit activation-energy tables.

The detailed observation showed that activation energies reported in the literature suffer from many experimental issues. First, the Arrhenius plots should fit at least 5 points (five temperatures, at least 40 °C range) instead of three only as in the majority of cases. Second, the viscosity vs. reciprocal temperature should be plotted at the relevant shear rates (PIM at 1000 s^{-1} and MEX at 100 s^{-1}) as done by Naranjo *et* al. [113], and this value must be stated in the paper. Furthermore, from a rheological point of view, evaluating activation energy at constant shear rate is not fully consistent for non-Newtonian systems. At a fixed shear rate, the corresponding shear stress changes with temperature, so the resulting activation energy of flow implicitly combines thermal effects with stress-induced structural changes in the compound. A more rigorous approach would be to determine activation energy at constant shear stress, which isolates the temperature dependence of viscosity at a fixed mechanical state of the material. For non-Newtonian fluids, the apparent activation energy obtained at constant stress is, in general, not equal to that obtained at constant shear rate; their ratio is related to the non-Newtonian (power-law) index, and thus reflects the degree of non-Newtonian behaviour. So far, the evaluations at constant shear stress are rather scarce. Karatas et al. [66] evaluated the effect of temperature on apparent viscosities of 50 vol% steatite feedstocks with binders containing polyethylene and three waxes (carnauba, bees wax and paraffin) under various shear stresses to be within the range of 25 to 99 kJ/mol, but each feedstock was evaluated at different shear stresses, thus the data are hardly comparable.

Furthermore, temperature sensitivity coefficients of feedstocks are also a function of pressure; those of binders are linearly increasing with pressure, and may increase up to three times in the pressure range from ambient to 50 MPa [120]. It is well known that pressure significantly affects the viscosity of MEX and PIM feedstocks, but rather surprisingly, there are only several studies, which investigate pressure-volume-temperature (PVT) behavior of PIM feedstocks to link pressure to shrinkage and final dimensions, and even less studies reporting pressure-dependent viscosity. Greene and Heaney [121] used a Tait-type PVT description of a PIM feedstock to correct molding shrinkage showing that increasing powder content lowers compressibility and reduces pressure sensitivity of specific volume, and that neglecting the feedstock PVT behavior leads to wrong dimensional predictions. Similar conclusions were drawn in later PVT-based studies on alumina [122], carbide feedstocks [123], barium titanate [124], aluminum nitride [125], silicon nitride [126], mullite-zirconia [18], Ni-based superalloy powder [127]. Fu *et* al. [128] employed PVT data to analyze the demolding failure of metal parts. Hausnerova *et* al. [123] demonstrated on various cemented carbide feedstocks (differing in particle size distribution and mean size) that the cause of the pressure dependence of the volumetric thermal expansion coefficients is linear, while the compressibility shows an exponential

cause and at high pressures it becomes almost pressure-independent. According to the Hashin and Shtrikman model [129] the stress transfer between the powder and the polymer binder can be neglected in the melting region, the measured data lies in between the mixing rule and Schapery's [130] lower boundary reflecting the weak bonding between the filler particles and the binder (Figure 7).

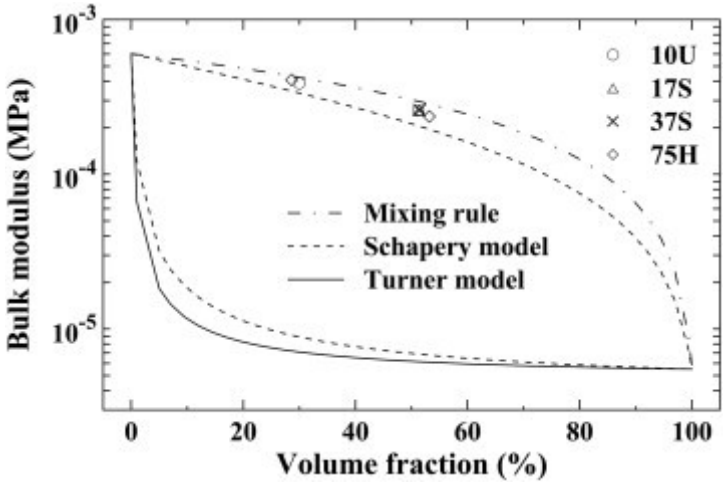

Figure 7 Bulk moduli of various carbide compounds varying in particle size distribution as a function of powder volume fraction. The dash-pot line represents the prediction according to the mixing rule, the dashed and full lines represent the boundaries of Schapery and Turner models, respectively (with permission from [123]).

Beyond classical confining-fluid and piston–die dilatometers, several groups have developed more process-relevant or mechanically simpler routes to obtain PVT data. Wang and co-workers [131] used production injection molding machines and instrumented molds to reverse determination of PVT behavior directly under realistic filling and packing conditions, thereby capturing effects of true molding pressures and cooling rates, which are difficult to reproduce in laboratory dilatometers. Rudolph *et* al. [132] implemented a squeeze-flow–type concept on a universal testing machine by placing a material charge between two coaxial pistons and recording force–displacement under controlled temperature, which allows extraction of specific volume and compressibility without a dedicated PVT apparatus. Conceptually similar to Rudolph’s squeeze-type setup has been recently used for a squeeze-flow based rheometry of carbon-fiber sheet molding compounds explicitly including PVT (compressibility) characterization [133]. Muranov *et* al. [134] designed an in-house plunger dilatometer for highly filled metal feedstocks and, in combination with DSC, showed that the melting and crystallization temperatures of polypropylene and wax in the binder shift substantially upwards when the pressure is increased by about 100 MPa; using the derived PVT and phase-transition data, they defined a practical processing window that supports processing of highly loaded mixtures with a minimized volumetric shrinkage and improved dimensional stability.

For MEX of highly filled feedstocks, the literature mainly incorporates pressure via pressure-drop and flow models (often including elongational effects) rather than through explicit pressure-dependent

viscosity coefficients, but it clearly recognizes that realistic prediction of extrusion behavior and printability requires coupling rheology with pressure evolution in the nozzle and die. Das *et* al. [135] as well as Brettmann *et* al. [136] emphasize that nozzle pressure, entrance pressure drop and pressure build-up along the hot end are crucial for print stability, layer thickness, and die swell.

Rane *et* al. [137] developed a pressure-drop model for twin-bore capillary rheometry for highly filled metal and ceramic feedstocks and showed that extrusion pressure cannot be predicted accurately without including elongational viscosity in addition to shear viscosity. It links measured pressures in the dies to rheological properties, demonstrating how process pressure reflects the combined shear and extensional response of the feedstock during material extrusion.

These studies clearly indicate that PVT behaviour and viscosity sensitivity to pressure are crucial for predicting shrinkage, residual stresses and demolding behaviour in PIM, and that similar systematic PVT data for MEX are essentially absent (pressure is usually considered only implicitly through extruder and nozzle pressure-drop measurements).

A direct determination of pressure-dependent viscosity requires a capillary rheometer equipped with an additional back-pressure unit that increases the hydrostatic pressure acting on the melt [138]. In this setup, a chamber is mounted at the capillary outlet and contains a needle valve, which is translated horizontally by a screw mechanism to adjust the backpressure imposed on the material during flow. With the help of such device, the effect of powder concentration as well as its features in terms of particle size distribution and shape can be evaluated. Pressure effect decreases with a loading level for low-to-moderate (up to 30 vol. %) powder concentrations [120] in accordance with German assumption [6]. However, at higher solid contents, the compounds appear more pressure-sensitive than the neat polymer binder itself [139]. This behavior suggests that, at powder loadings relevant for PIM and MEX, the compressibility of the particle network and its internal structure starts to play a dominant role, whereas at low to moderate powder fractions the pressure response is controlled mainly by the binder.

Further, the pressure coefficient of viscosity also varies in a systematic way with powder properties (particle size, size distribution, morphology): finer or more irregular powders tend to produce higher absolute viscosities, but their viscosity often changes less with pressure; pressure sensitivity can be tuned by adjusting powder characteristics [140]. To date, however, such pressure-dependent viscosity data exist only for a limited number of feedstocks and have not yet been integrated into standard simulation workflows; recent measurement-technique reviews summarize in-mold PVT and pressure–specific-volume measurements as emerging, non-standard tools for process-driven characterization [141].

Chapter summary:

- Classical flow models (power law, Carreau, Cross) developed for fitting pure polymer melts do not capture yield stress or wall slip, which are typical for highly filled MEX/PIM compounds. As a

consequence, powder-binder segregation, near wall defects and flow instabilities are not intercepted with rheological testing.

- Master curves approach provide a compact and efficient way to describe shear viscosity dependence on feedstock composition with an accuracy not exceeding an experimental error.
- Activation energy can serve as an indicator of both the critical powder loading (turn from activation energy decreasing into increasing upon adding powders) and the onset of flow instabilities (falling out from linear Arrhenius trend). However, it must be evaluated correctly within at least a 40 °C range and preferably at constant shear stress.
- Pressure strongly affects viscosity, yet pressure-dependent viscosity has been measured only for a few PIM systems and is not integrated into flow simulations. Existing data suggest that pressure effects become increasingly important at powder loadings relevant for MEX/PIM, where compressibility of the particle network and its internal structure overtake a dominant role of a binder.

4 Rheology as a predictive tool for flow instabilities, segregation, and defect mitigation

Rheological characterization of highly filled MEX and PIM feedstocks is not only a tool for basic material description but also a powerful means to identify, understand, and mitigate processing defects such as flow instabilities and powder/binder segregation. As already stressed, PIM/MEX compounds exhibit complex, strongly non-Newtonian flow because powder contents are close to the critical packing limit. Under such conditions, even small changes in local shear rate, pressure, or geometry can trigger instabilities that are still not fully understood and that often manifest as phase separation between powder and multicomponent binder, leading to defects as porosity and/or cracks on the final sintered parts, which are unacceptable in highly demanding applications as aerospace, automotive, or medical sectors. A key question is therefore whether measured rheological parameters can be used to predict or even prevent such defects.

Powder-binder separation during injection molding results in uneven shrinkage [142], and represents pathways for reducing energy consumption and product failure. Experimental evidence shows that powder characteristics (size distribution, shape, surface) and process conditions have a decisive influence on both flow behavior and segregation tendency. Coarser, spherical powders can be easily moldable but also more prone to flow instabilities, while wide size distributions promote structural inhomogeneities in the products. Attempts to map flow-induced segregation using DSC [143], X-ray tomography [144-146] synchrotron microtomography in complex molds [147], and EDX/SEM combined with analytical tools [148, 149] have demonstrated particle redistribution during Poiseuille flow. These techniques provide valuable qualitative and sometimes quantitative insight into segregation patterns but are experimentally demanding and often not suited for a routine process optimization. Against these efforts, rheological methods offer a complementary route to reduce or even eliminate the segregation.

Wall-slip, emerging as a rheological phenomenon that can be directly linked to powder–binder separation, can be measured on a standard capillary rheometer. Empirical evidences suggest that a controlled slip can mitigate powder-binder segregation. When a thin, low-viscosity binder layer forms at the wall and allows the bulk suspension to slide, the shear-rate gradients within the particulate core are reduced; this weakens the driving force for particle migration and can suppress powder–binder separation. Online slit-die rheometry of commercial and in-house PIM feedstocks showed that essentially all highly filled systems exhibit wall slip under processing-like conditions, and that the slip velocity depends on binder type, powder characteristics [150], and the surface properties [151].

The thickness of the polymer layer created near the channel wall during slippage is proportional to the square root of the wall slip velocity [152,153]. From a few available studies [80,81], the molecular weight of a binder seems to have an effect on the thickness of this polymer layer; for feedstocks containing lower molecular weight it is higher than for higher molecular weight feedstocks. The role of the powder chemistry also remains rather unexplored. It has been shown that stainless steel is more prone to a wall slip than Al_2O_3 [154], and interestingly, the tendency of Al_2O_3 feedstock to wall slip is less pronounced than for ZrO_2 compounds [151], although their surface characteristics (surface energies) are fairly similar (44 and 47 J/m^2 for ZrO_2 and Al_2O_3, respectively [86]). However, even if the rheological conditions and binder composition are kept the same, the effect of powder chemistry cannot be separated from their features which are the crucial for wall slip. It has been shown that the slip velocity can be substantially reduced by tailoring a powder particle size distribution towards smaller particles fractions [150].

The factor, which complicates wall slip evaluation is that the obtained slip velocities are highly affected by the measurement arrangement. It has been demonstrated that the velocity decreases with increasing channel size and surface roughness, especially if surface irregularities are higher than polymer layers formed at the flow channel walls [151, 155, 156]. At present, the heterogenous surfaces can be precisely quantified and statistically analysed with the help of cluster analysis combined with single-layer neural networks [157, 158].

Further, a capillary entrance angle in a capillary rheometry is another critical parameter for both reliable slip quantification and realistic representation of process conditions. Flat 180° dies systematically overestimate slip velocities and promote powder–binder separation at the die entrance, whereas 90° conical dies provide slip–stress relations that align with established linear scaling for highly filled feedstocks and better simulate the flow encountered in real molds [159]. Hasib *et* al. [160] correlated filament extrudability and quality of printed parts with rheology and specifically discuss deviations between capillary and rotational data at high shear rates attributed to wall slip in capillaries, highlighting that unrecognized slip can lead to underestimation of the true viscosity and misinterpretation of processing windows. To fully eliminate slip from the rheological measurements, multi-scale velocimetry must be employed as proposed by Haavisto *et* al. [161] combining Doppler

optical coherence tomography with magnetic resonance imaging or ultrasound velocity profiling to investigate a pipe flow of complex materials.

Mannschatz *et* al. [162] reported that separation of powder and binder within feedstock is most severe near high shear-rate gradients and dead zones, consistent with the slip-layer concept. A later numerical study of special flow situations in PIM explicitly concludes that wall slip reduces powder–binder segregation by lowering shear-rate gradients and thus the driving force for migration [163].

The influence of the wall slip on the filament extrudability and windability was demonstrated by Hasib *et* al. [160] for PLA/Ni–Cu powder feedstocks. LeBlanc *et* al. [164] and Saidy *et* al. [165] associated the wall slip with extrudate distortions and other extrusion defects, resulting in a reduction of an adhesive strength between deposited filaments. Maciel *et* al. [166] linked the areas that appear sheared in the angular direction of the extrudate to the slip effects. Vadodaria *et* al. [167] reported strongly heterogeneous velocity profiles across the measurement gap for cellulose-based systems widely used in 3D printing, attributing them to discontinuous shear gradients caused by wall slip.

To sum up, it has been demonstrated that some degree of slip can be beneficial in reducing powder migration and powder-binder segregation in regions of high shear, but excessive or poorly controlled slip can also produce binder-rich surface layers and change local stress states, which may compromise bonding and green-body integrity in PIM. The MEX-related observations underline that, while slip can help to reduce pressure and avoid clogging, it can simultaneously promote surface defects, interfacial weakness and heterogeneous filament structure if it is not balanced by sufficient bulk cohesion.

Further, following the work of Haavisto *et* al. [161], several studies [168-171] have examined the interplay between yield stress and wall shear stress in the presence of slip, indicating that when the wall shear stress exceeds the material's yield stress, phase separation and non-uniform print quality are likely to appear. Delime and Moan [172] attributes the separation to a breakdown of Brownian motion near the walls, further intensified by shear-rate gradients that promote particle collisions which were experimentally confirmed by Lam *et* al. [173]. This suggests that the wall shear stress/yield stress ratio can serve as a key control parameter: if wall stresses remain comparable to or below the yield stress, the material flows without separation.

Kukla *et* al. [174] pointed out that the yield stress is a parameter strongly affecting flow behavior of MEX (and PIM) compounds, and that quantifying yield stress must be done carefully because the obtained values depend on the analytical technique used. They compared yield stresses measured with a control-stress rheometer (CSS) with measurements made on a slit-die rheometer in a controlled shear rate mode, and found CSS more sensitive providing more accurate data. In their review [103], they further emphasize that realistic modelling must include a yield stress to capture the onset of flow and green-body stability, especially near weld lines and thin sections. Further, Marnot *et* al. [65] pointed out that higher static yield stress improves buildability and shape retention in MEX, but at the cost of higher extrusion pressure; a balance must be found between pumpability/extrudability and the yield

stress needed to avoid slumping or spreading after deposition. Naranjo *et* al. [113] found for hybrid MIM/MEX feedstocks based on 17-4PH stainless steel powder that yield stress, together with viscosity and activation energy, sets limits on suitable printing speeds and temperatures to avoid either under-extrusion (too high yield) or filament sagging and interlayer smearing (too low yield). Poslinski proposed a theoretical expression which directly relates the solid fraction to the yield stress [175]. It indicates that the magnitude of the yield stress increases with the increasing volume fraction of the powder, decreasing size of the particles and increasing interparticle surface potential [176, 177], which is not surprising as it is defined as the force per unit area necessary to overcome interactions within interparticle network formed in a highly filled compound.

Finally, it should be noted that in oscillatory rheology, some authors loosely refer to the crossover between the storage modulus and the loss modulus in an amplitude sweep as a yield point, although this crossover merely marks the switch from elastic-dominant to viscous-dominant behavior. As an example, Eickhoff *et* al. [178] adopts this nomenclature in a comprehensive Ti-6Al-4V MEX feedstock study, call a distinct region where the storage modulus clearly dominates the loss modulus up to a well-defined crossover as a yield point, and found it beneficial for MEX, because in that regime small deformations during deposition do not remelt or destabilize the previously printed layer, and thus preserve surface stability. In their Ti-6Al-4V feedstocks, however, no such crossover is observed within the measured range, so the material remains predominantly viscous, which they identify as unfavorable for maintaining structural integrity during layer-on-layer deposition.

Chapter summary:

- Rheology can provide parameters (wall slip, yield stress) which are linked to the filament extrudability and windability defects in MEX, and flow instabilities and powder-binder segregation in PIM.
- Both, wall slip and yield stress are very sensitive to the experimental arrangement. A control-stress rheometer is recommended for precise evaluation of yield stress, and a capillary rheometer with conical die is preferred for wall slip determination.
- Flow simulations and modelling must include yield stress and slip velocity to capture an onset of flow and molded/extruded part stability, especially near weld lines and thin sections.
- Practice-relevant advice based on empirical findings from processing of highly demanding parts: a temperature-controlled slip and nearly plug flow, often results in defect-free parts due to the reduction of the particle migration out of high shear regions.

Conclusion

Rheology is a routine approach for understanding the flow behaviour of highly filled MEX and PIM feedstocks, yet its potential as a functional process tool is still far from fully exploited. Existing studies provide a wealth of viscosity curves, model fits, and case specific observations; however, systematic,

generally applicable links between measured rheological parameters and robust processing windows remain rare.

This review identifies wall slip velocity, yield stress, activation energy of flow, and pressure dependent viscosity as particularly promising quantities, because each can be directly related to critical failure modes such as powder–binder segregation, flow instabilities, dimensional tolerances failure, and loss of a green body integrity. At the same time, several widely used practices deserve reconsideration: evaluating activation energy exclusively at constant shear rate conflates thermal and structural effects, applying classic shear thinning models (power law, Carreau, Cross) to feedstocks near the packing limit ignores yield stress and wall slip, and neglecting pressure sensitivity leads to unrealistic flow simulations.

We therefore propose that the next step for rheology in MEX and PIM is not primarily to refine fits of classical models to more data, but rather to:

- establish a limited set of physically meaningful, experimentally accessible rheological parameters as standard reporting quantities across studies;
- integrate these parameters into flow simulations and defect prediction criteria rather than treating them as isolated material descriptors;
- develop transferable, composition-based tools - such as master curves and quantitative binder interaction maps - that allow to anticipate processing behaviour before committing to full scale trials.

In our view, this translates into development of feedstocks which exhibit well-defined wall-slip, yield stresses, intercept their pressure sensitivity and eliminate abrupt viscosity changes with shear rate or time, rather than merely matching a target low viscosity and power-law index values. If this shift from descriptive viscosity curves toward process relevant rheological metrics is achieved, rheological characterization will become a practical design tool for engineers working with the increasingly merged MEX/PIM technologies.

Funding: This publication was created as part of the implementation of the project Testing laboratory for the implementation of sustainable and resilient technologies, reg. number CZ.02.01.01/00/23_021/0010411, co-financed by the European Union under the OP Jan Amos Comenius.

CRediT Author Statement

D.E. – investigation, resources, visualization, writing - original draft, M.N. – resources; B.H.: conceptualization, supervision, writing - review and editing, funding acquisition, project administration; All authors have read and agreed to the content of the manuscript.

Declaration of interests

The authors have no conflicts to disclose.

Data Aviability

No data were created within this paper.

References

1. Q. He, J. Jiang, X. Yang, L. Zhang, Z. Zhou, Y. Zhong, Z. Shen, Additive manufacturing of dense zirconia ceramics by fused deposition modeling via screw extrusion, J. Eur. Ceram. Soc., 41 (2021), 1033–1040, https://doi.org/10.1016/j.jeurceramsoc.2020.09.018.
2. M. Novak, B. Hausnerova, V. Pata, D. Sanetrnik, On the possibilities of merging additive manufacturing and powder injection molding in the production of metal parts, Rapid Prototyp. J., 30 (2024), 50–58, https://doi.org/10.1108/RPJ-02-2023-0047.
3. A. M. Hadian, M. Fricke, A. Liersch, F. Clemens, Material extrusion additive manufacturing of zirconia parts using powder injection molding feedstock compositions, Addit. Manuf., 57 (2022), 102966, https://doi.org/10.1016/j.addma.2022.102966.
4. T. Shen, H. Xiong, Z. Li, L. Zhang, K. Zhou, Fused deposition fabrication of high-quality zirconia ceramics using granular feedstock, Ceram. Int., 47 (2021), 34352–34360, https://doi.org/10.1016/j.ceramint.2021.08.348.
5. K. Rane, M. A. Farid, W. Hassan, M. Strano, Effect of printing parameters on mechanical properties of extrusion-based additively manufactured ceramic parts, Ceram. Int., 47 (2021), 12189–12198, https://doi.org/10.1016/j.ceramint.2021.01.066.
6. R. M. German, Powder Injection Molding, Metal Powder Industries Federation, Princeton, NJ, 1990.
7. B. Hausnerova, Rheological characterization of powder injection molding compounds, Polimery, 55 (2010), 3–11, https://doi.org/10.14314/polimery.2010.003.
8. R. M. German, Injection Molding of Metals and Ceramics, Metal Powder Industries Federation, Princeton, NJ, 1997.
9. M. S. Ramalingam, K. N. Chaithanya Kumar, S. Sharma, S. S. Joshi, N. B. Dahotre, Binder jet additive manufacturing: a review of modelling approaches and experimental observations on green part printing, Virtual Phys. Prototyp., 20 (2025), e2547091, https://doi.org/10.1080/17452759.2025.2547091.
10. K. S. Shahed, G. Manogharan, Powder-binder interaction in binder jetting process: a simulation study on bimodal powders, in: Proc. ASME 2023 Int. Manuf. Sci. Eng. Conf. (MSEC2023), ASME, New York, NY, 2023, https://doi.org/10.1115/MSEC2023-104366.
11. V. Momeni, M. Hufnagl, Z. Shahroodi, J. Gonzalez-Gutierrez, S. Schuschnigg, C. Kukla, C. Holzer, Research progress on low-pressure powder injection molding, Materials, 16 (2022), 379, https://doi.org/10.3390/ma16010379.
12. L. Urtekin, A. Taşkın, Ti–6Al–4V alloy cortical bone screw production by powder injection molding method, Mater. Express, 7 (2017), 245–252, https://doi.org/10.1166/mex.2017.1378.
13. R. Côté, M. Azzouni, V. Demers, Impact of binder constituents on the moldability of titanium-based feedstocks used in low-pressure powder injection molding, Powder Technol., 381 (2021), 255–268, https://doi.org/10.1016/j.powtec.2020.12.008.
14. X. Kong, T. Barriere, J. C. Gelin, Determination of critical and optimal powder loadings for 316L fine stainless steel feedstocks for micro-powder injection molding, J. Mater. Process. Technol., 212 (2012), 2173–2182, https://doi.org/10.1016/j.jmatprotec.2012.05.023.
15. L. Liu, X. L. Ni, H. Q. Yin, X. H. Qu, Mouldability of various zirconia micro gears in micro powder injection moulding, J. Eur. Ceram. Soc., 35 (2015), 171–177, https://doi.org/10.1016/j.jeurceramsoc.2014.07.027.
16. P. Thomas-Vielma, A. Cervera, B. Levenfeld, A. Várez, Production of alumina parts by powder injection molding with a binder system based on high density polyethylene, J. Eur. Ceram. Soc., 28 (2008), 763–771, https://doi.org/10.1016/j.jeurceramsoc.2007.08.004.
17. G. Aggarwal, S. J. Park, I. Smid, Development of niobium powder injection molding: Part I. Feedstock and injection molding, Int. J. Refract. Met. Hard Mater., 24 (2006), 253–262, https://doi.org/10.1016/j.ijrmhm.2005.06.003.

18. R. Martin, M. Vick, M. Kelly, J. P. de Souza, R. K. Enneti, S. V. Atre, Powder injection molding of a mullite–zirconia composite, J. Mater. Res. Technol., 2 (2013), 263–268, https://doi.org/10.1016/j.jmrt.2013.03.014.
19. J. Ma, M. Qin, L. Zhang, L. Tian, R. Li, P. Chen, X. Qu, Effect of ball milling on the rheology and particle characteristics of Fe–50%Ni powder injection molding feedstock, J. Alloys Compd., 590 (2014), 41–45, https://doi.org/10.1016/j.jallcom.2013.12.080.
20. N. Mukund, B. Hausnerova, Variation in particle size fraction to optimize metal injection molding of water atomized 17–4PH stainless steel feedstocks, Powder Technol., 368 (2020), 130–136, https://doi.org/10.1016/j.powtec.2020.04.058.
21. S. Y. Heng, M. R. Raza, N. Muhamad, A. B. Sulong, A. Fayyaz, Micro-powder injection molding (μPIM) of tungsten carbide, Int. J. Refract. Met. Hard Mater., 45 (2014), 189–195, https://doi.org/10.1016/j.ijrmhm.2014.04.012.
22. S. Yang, R. Zhang, X. Qu, X-ray tomographic analysis of powder-binder separation in SiC green body, J. Eur. Ceram. Soc., 33 (2013), 2935–2941, https://doi.org/10.1016/j.jeurceramsoc.2013.06.011.
23. P. Chakartnarodom, N. Chuankrerkkul, Statistical analysis of binder behavior during debinding step in powder injection molding (PIM), Adv. Mater. Res., 970 (2014), 172–176, https://doi.org/10.4028/www.scientific.net/AMR.970.172.
24. N. Chuankrerkkul, H. A. Davies, P. F. Messer, Application of PEG/PMMA binder for powder injection moulding of hardmetals, Mater. Sci. Forum, 561–565 (2007), 953–956, https://doi.org/10.4028/www.scientific.net/MSF.561-565.953.
25. H. I. Bakan, Y. Jumadi, P. F. Messer, H. A. Davies, B. Ellis, Study of processing parameters for MIM feedstock based on composite PEG-PMMA binder, Powder Metall., 41 (1998), 289–291, https://doi.org/10.1179/pom.1998.41.4.289.
26. E. Hnátková, B. Hausnerova, A. Hales, L. Jiranek, F. Derguti, I. Todd, Processing of MIM feedstocks based on Inconel 718 powder and partially water-soluble binder varying in PEG molecular weight, Powder Technol., 322 (2017), 439–446, https://doi.org/10.1016/j.powtec.2017.09.029.
27. M. Y. Anwar, P. F. Messer, B. Ellis, H. A. Davies, Injection moulding of 316L stainless steel powder using novel binder system, Powder Metall., 38 (1995), 113–119, https://doi.org/10.1179/pom.1995.38.2.113.
28. V. A. Krauss, A. A. M. Oliveira, A. N. Klein, H. A. Al-Qureshi, M. C. Fredel, A model for PEG removal from alumina injection moulded parts by solvent debinding, J. Mater. Process. Technol., 182 (2007), 268–273, https://doi.org/10.1016/j.jmatprotec.2006.08.004.
29. B. Hausnerova, M. Novak, Environmentally efficient 316L stainless steel feedstocks for powder injection molding, Polymers, 12 (2020), 1296, https://doi.org/10.3390/polym12061296.
30. B. Hausnerova, I. Kuritka, D. Bleyan, Polyolefin backbone substitution in binders for low temperature powder injection moulding feedstocks, Molecules, 19 (2014), 2748–2760, https://doi.org/10.3390/molecules19032748.
31. S. Hwang, E. I. Reyes, K. Moon, R. C. Rumpf, N. S. Kim, Thermo-mechanical characterization of metal/polymer composite filaments and printing parameter study for fused deposition modeling in the 3D printing process, J. Electron. Mater., 44 (2015), 771–777, https://doi.org/10.1007/s11664-014-3425-6.
32. L. Ren, X. Zhou, Z. Song, C. Zhao, Q. Liu, J. Xue, X. Li, Process parameter optimization of extrusion-based 3D metal printing utilizing PW–LDPE–SA binder system, Materials, 10 (2017), 305, https://doi.org/10.3390/ma10030305.
33. M. Nötzel, R. Eickhoff, T. Hanemann, Fused filament fabrication of small ceramic components, Materials, 11 (2018), 1463, https://doi.org/10.3390/ma11081463.
34. N. Sa'ude, M. Ibrahim, M. H. I. Ibrahim, Mechanical properties of highly filled iron-ABS composites in injection molding for FDM wire filament, Mater. Sci. Forum, 773–774 (2014), 448–453, https://doi.org/10.4028/www.scientific.net/MSF.773-774.448.
35. N. Sa'ude, S. H. Masood, M. Nikzad, M. Ibrahim, M. H. I. Ibrahim, Dynamic mechanical properties of copper-ABS composites for FDM feedstock, Int. J. Eng. Res. Appl., 3 (2013), 3, 1257–1263.

36. S. H. Masood, W. Q. Song, Development of new metal/polymer materials for rapid tooling using fused deposition modelling, Mater. Des., 25 (2004), 7, 587–594, https://doi.org/10.1016/j.matdes.2004.02.009.
37. M. K. Agarwala, R. van Weeren, A. Bandyopadhyay, A. Safari, S. C. Danforth, W. R. Priedeman, Filament feed materials for fused deposition processing of ceramics and metals, in: Proc. Solid Freeform Fabrication Symposium, Austin, TX, 1996, pp. 451–458, https://doi.org/10.15781/T2GX45D8J.
38. M. K. Agarwala, R. van Weeren, A. Bandyopadhyay, P. J. Whalen, A. Safari, S. C. Danforth, Fused deposition of ceramics and metals: An overview, in: Proc. Solid Freeform Fabrication Symposium, Austin, TX, 1996, pp. 385–395, https://doi.org/10.15781/T2NK36Q96.
39. S. Onagoruwa, S. Bose, A. Bandyopadhyay, Fused deposition of ceramics (FDC) and composites, in: Proc. Solid Freeform Fabrication Symposium, Austin, TX, 2001, pp. 224–231, https://doi.org/10.26153/tsw/3267.
40. A. Bandyopadhyay, K. Das, J. Marusich, S. Onagoruwa, Application of fused deposition in controlled microstructure metal-ceramic composites, Rapid Prototyp. J., 12 (2006), 3, 121–128, https://doi.org/10.1108/13552540610670690.
41. M. K. Agarwala, R. van Weeren, R. Vaidyanathan, A. Bandyopadhyay, G. Carrasquillo, V. Jamalabad, N. Langrana, A. Safari, S. H. Garofalini, S. C. Danforth, J. Burlew, R. Donaldson, P. Whalen, C. Ballard, Structural ceramics by fused deposition of ceramics, in: Proc. Solid Freeform Fabrication Symposium, Austin, TX, 1995, pp. 1–8, https://doi.org/10.15781/T2N873J4Q.
42. T. F. McNulty, D. J. Shanefield, S. C. Danforth, A. Safari, Dispersion of lead zirconate titanate for fused deposition of ceramics, J. Am. Ceram. Soc., 82 (1999), 7, 1757–1760, https://doi.org/10.1111/j.1151-2916.1999.tb01996.x.
43. T. F. McNulty, F. Mohammadi, A. Bandyopadhyay, D. J. Shanefield, S. C. Danforth, A. Safari, Development of a binder formulation for fused deposition of ceramics, Rapid Prototyp. J., 4 (1998), 4, 144–150, https://doi.org/10.1108/13552549810239012.
44. C. Kukla, J. Gonzalez-Gutierrez, S. Cano Cano, S. Hampel, C. Burkhardt, T. Moritz, C. Holzer, Fused filament fabrication (FFF) of PIM feedstocks, in: Proc. VI Congreso Nacional de Pulvimetalurgia y I Congreso Iberoamericano de Pulvimetalurgia, (2017), 1–6. https://www.researchgate.net/publication/317845478_FUSED_FILAMENT_FABRICATION_FFF_OF_PIM_FEEDSTOCKS
45. J. Gonzalez-Gutierrez, R. Guráň, M. Spörk, C. Holzer, D. Godec, C. Kukla, 3D printing conditions determination for feedstock used in fused filament fabrication (FFF) of 17-4PH stainless steel parts, Metalurgija, 57 (2018), 117–120. https://www.researchgate.net/publication/321267480_3D_printing_conditions_determination_for_feedstock_used_in_fused_filament_fabrication_FFF_of_17-4PH_stainless_steel_parts
46. C. Kukla, I. Duretek, S. Schuschnigg, J. Gonzalez Gutierrez, C. Holzer, Properties for PIM feedstocks used in fused filament fabrication, in: F. Petzoldt (Ed.), Proc. World PM2016 Congress & Exhibition, European Powder Metallurgy Association, (2016), 1–5. https://pure.unileoben.ac.at/en/publications/properties-for-pim-feedstocks-used-in-fused-filament-fabrication
47. C. Kukla, J. Gonzalez-Gutierrez, C. Burkhardt, O. Weber, and C. Holzer, The Production of Magnets by FFF - Fused Filament Fabrication, in Euro PM2017 Congress & Exhibition, European Powder Metallurgy Association, (2017), 1-6. https://www.researchgate.net/publication/321242756_The_Production_of_Magnets_by_FFF_-_Fused_Filament_Fabrication#fullTextFileContent
48. J. Gonzalez Gutierrez, S. Cano, S. Schuschnigg, C. Kukla, J. Sapkota, C. Holzer, Additive manufacturing of metallic and ceramic components by the material extrusion of highly filled polymers: A review and future perspectives, Materials, 11 (2018), 840, https://doi.org/10.3390/ma11050840.
49. C. Kukla, S. Cano, D. Kaylani, S. Schuschnigg, C. Holzer, J. Gonzalez Gutierrez, Debinding behaviour of feedstock for material extrusion additive manufacturing of zirconia, Powder Metall., 62 (2019), 3, 196–204, https://doi.org/10.1080/00325899.2019.1616139.

50. C. Holzer, C. Kukla, I. Duretek, S. Schuschnigg, J. Gonzalez Gutierrez, Effect of particle size on the properties of highly filled polymers for fused filament fabrication, in: 32nd Int. Conf. of the Polymer Processing Society, 2016, https://doi.org/10.1063/1.5016795.
51. S. Riecker, J. Clouse, T. Studnitzky, O. Andersen, B. Kieback, Fused deposition modeling – Opportunities for cheap metal AM, in: Euro PM2016 Congress & Exhibition, 2016, 1–6. https://www.researchgate.net/publication/340681726_Fused_deposition_modeling-opportunities_for_cheap_metal_AM
52. A. M. Abdullah, T. N. A. Tuan Rahim, D. Mohamad, H. M. Akil, Z. A. Rajion, Mechanical and physical properties of highly ZrO2/β TCP filled polyamide 12 prepared via fused deposition modelling (FDM) 3D printer for potential craniofacial reconstruction application, Mater. Lett., 189 (2017), 307–309, https://doi.org/10.1016/j.matlet.2016.11.052.
53. S. Cano, J. Gonzalez Gutierrez, J. Sapkota, M. Spoerk, F. Arbeiter, S. Schuschnigg, C. Holzer, C. Kukla, Additive manufacturing of zirconia parts by fused filament fabrication and solvent debinding: Selection of binder formulation, Addit. Manuf., 26 (2019), 117–128, https://doi.org/10.1016/j.addma.2019.01.001.
54. H. Giberti, M. Strano, M. Annoni, An innovative machine for fused deposition modeling of metals and advanced ceramics, MATEC Web Conf., 43 (2016), 03003, https://doi.org/10.1051/matecconf/20164303003.
55. G. Farrow, A. Conciatori, Polyacetal binders for injection moulding of ceramics, DE3477767D1, 1989.
56. H. J. Sterzel, J. Ter Maat, J. Ebenhoech, M. Meyer, Thermoplastic materials for the production of ceramic moldings, US5145900A, 1992.
57. J. C. LaSalle, M. Behi, G. A. Glandz, J. V. Burlew, Aqueous nonferrous feedstock material for injection molding, US20020096016A1, 2002.
58. R. Wiech Jr., Manufacture of parts from particulate material, US4197118A, 1980.
59. X. Yang, R. J. Petcavich, Powder and binder systems for use in metal and ceramic powder injection molding, US6008281A, 1999.
60. P. Daute, M. Jaeckel, J. Waldmann, Sinterable feedstock for use in 3D printing devices, US10737480B2, 2020.
61. K. Heikkilä, Surface modified particulate and sintered or injection molded products, US10052691B2, 2018.
62. N. Nestle, M. C. Hermant, K. Schmidt, Mixture for use in a fused filament fabrication process, WO2016012486A1, 2016.
63. M. T. Zaky, F. S. Soliman, A. S. Farag, Influence of paraffin wax characteristics on the formulation of wax based binders and their debinding from green molded parts using two comparative techniques, J. Mater. Process. Technol., 209 (2009), 18–19, 5981–5989, https://doi.org/10.1016/j.jmatprotec.2009.07.018.
64. B. Hausnerova, P. Saha, J. Kubat, T. Kitano, J. Becker, Rheological behaviour of hard metal carbide powder suspensions at high shear rates, J. Polym. Eng., 20 (2000), 4, https://doi.org/10.1515/POLYENG.2000.20.4.237.
65. A. Marnot, K. Koube, S. Jang, N. Thadhani, J. Kacher, B. Brettmann, Material extrusion additive manufacturing of high particle loaded suspensions: A review of materials, processes and challenges, Virtual Phys. Prototyp., 18 (2023), 1, https://doi.org/10.1080/17452759.2023.2279149.
66. C. Karataş, A. Köçer, H. I. Ünal, S. Sarıtaş, Rheological properties of feedstocks prepared with steatite powder and polyethylene based thermoplastic binders, J. Mater. Process. Technol., 152 (2004), 1, 77–83, https://doi.org/10.1016/j.jmatprotec.2004.03.009.
67. N. Muranov, V. R. Lysenko, M. A. Kocharov, Rheological behavior features of feedstocks with a two component wax–polyolefin binder compared to analogs based on polyoxymethylene, J. Compos. Sci., 8 (2024), 6, 199, https://doi.org/10.3390/jcs8060199.
68. F. Fareh, V. Demers, N. R. Demarquette, S. Turenne, O. Scalzo, Influence of segregation on rheological properties of wax based feedstocks, Powder Technol., 320 (2017), 273–284, https://doi.org/10.1016/j.powtec.2017.07.056.
69. B. Hausnerova, P. Saha, J. Kubat, Capillary flow of hard metal carbide powder compounds, Int. Polym. Process., 14 (1999), 3, 254–260, https://doi.org/10.3139/217.1556.

70. A. N. bin Abdullah, N. binti Johari, M. J. bin Suleiman Ahmad, R. Ibrahim, A. R. A. Talib, Analysis of the rheological behavior and stability of Inconel 718 powder injection molding (PIM) feedstock, Adv. Mater. Res., 879 (2014), 63–72, https://doi.org/10.4028/www.scientific.net/AMR.879.63.
71. J. M. Park, J. S. Han, C. W. Gal, J. W. Oh, K. H. Kate, S. V. Atre, Y. Kim, S. J. Park, Effect of binder composition on rheological behavior of PMN PZT ceramic feedstock, Powder Technol., 330 (2018), 19–26, https://doi.org/10.1016/j.powtec.2018.02.027.
72. T. Forstner, S. Cholewa, D. Drummer, Influence of wax addition on feedstock processing behavior in additive manufacturing of metals by material extrusion, Prog. Addit. Manuf., 9 (2024), 3, 625–632, https://doi.org/10.1007/s40964-024-00671-4.
73. L. Urtekin, I. Uslan, B. Tuç, Investigation of properties of powder injection molded steatites, J. Mater. Eng. Perform., 21 (2012), 358–365, https://doi.org/10.1007/s11665-011-9901-8.
74. K. C. Hsu, C. C. Lin, G. M. Lo, Effect of wax composition on injection moulding of 304L stainless steel powder, Powder Metall., 37 (1994), 4, 272–276, https://doi.org/10.1179/pom.1994.37.4.272.
75. W. J. Tseng, Influence of surfactant on rheological behaviors of injection molded alumina suspensions, Mater. Sci. Eng. A, 289 (2000), 1–2, 116–122, https://doi.org/10.1016/S0921-5093(00)00895-9.
76. V. Momeni, [doplnit všechny autory], Binder system composition on the rheological and magnetic properties of Nd Fe B feedstocks for metal injection molding, Appl. Sci., 14 (2024), 13, 5638, https://doi.org/10.3390/app14135638.
77. R. Eickhoff, S. Antusch, D. Nötzel, T. Hanemann, New partially water soluble feedstocks for additive manufacturing of Ti6Al4V parts by material extrusion, Materials, 16 (2023), 8, 3162, https://doi.org/10.3390/ma16083162.
78. M. Elbadawi, Rheological and mechanical investigation into the effect of different molecular weight poly(ethylene glycol)s on polycaprolactone ciprofloxacin filaments, ACS Omega, 4 (2019), 3, 5412–5423, https://doi.org/10.1021/acsomega.8b03057.
79. M. D. Hayat, G. Wen, M. F. Zulkifli, P. Cao, Effect of PEG molecular weight on rheological properties of Ti MIM feedstocks and water debinding behaviour, Powder Technol., 270 (2015), 296–301, https://doi.org/10.1016/j.powtec.2014.10.035.
80. W. W. Yang, K. Y. Yang, M. H. Hon, Effects of PEG molecular weights on rheological behavior of alumina injection molding feedstocks, Mater. Chem. Phys., 78 (2003), 2, 416–424, https://doi.org/10.1016/S0254-0584(02)00203-1.
81. J. Gonzalez Gutierrez, P. Oblak, B. S. von Bernstorff, I. Emri, Improving powder injection moulding by modifying binder viscosity through different molecular weight variations, in: Proc. 11th Global Conf. on Sustainable Manufacturing – Innovative Solutions, G. Seliger (Ed.), Universitätsverlag der TU Berlin, Berlin, 2013, pp. 393–397. ISBN 978 3 7983 2609 5.
82. F. Chen, M. P. Wolcott, Miscibility studies of paraffin/polyethylene blends as form stable phase change materials, Eur. Polym. J., 52 (2014), 44–52, https://doi.org/10.1016/j.eurpolymj.2013.09.027.
83. Y. N. Sudhakar, M. Selvakumar, Miscibility of chitosan and poly(ethyleneglycol) blends in buffer solution, e Polym., 12 (2012), 1, 1037, https://doi.org/10.1515/epoly.2012.12.1.1037.
84. A. H. Doulabi, H. Mirzadeh, M. Imani, Miscibility study of chitosan/polyethylene glycol fumarate blends in dilute solutions, J. Appl. Polym. Sci., 127 (2013), 5, 3514–3521, https://doi.org/10.1002/app.37637.
85. I. O. Ucar, M. D. Doganci, C. E. Cansoy, H. Y. Erbil, I. Avramova, S. Suzer, Combined XPS and contact angle studies of ethylene vinyl acetate and polyvinyl acetate blends, Appl. Surf. Sci., 257 (2011), 22, 9587–9594, https://doi.org/10.1016/j.apsusc.2011.06.070.
86. B. Hausnerova, D. Bleyan, V. Kasparkova, V. Pata, Surface adhesion between ceramic injection molding feedstocks and processing tools, Ceram. Int., 42 (2016), 1, 460–465, https://doi.org/10.1016/j.ceramint.2015.08.132.
87. T. Cheny, C. Colin, S. Gailliègue, P. Calves, B. Verquin, Understanding drying dynamics in binder jetting: Development of a physical model for improved selection of drying parameters and better control of binder saturation, Addit. Manuf., 106 (2025), 104798, https://doi.org/10.1016/j.addma.2025.104798.

88. D. Bleyan, B. Hausnerova, P. Svoboda, The development of powder injection moulding binders: A quantification of individual components' interactions, Powder Technol., 286 (2015), 84–89, https://doi.org/10.1016/j.powtec.2015.07.046.
89. D. Bleyan, P. Svoboda, B. Hausnerova, Specific interactions of low molecular weight analogues of carnauba wax and polyethylene glycol binders of ceramic injection moulding feedstocks, Ceram. Int., 41 (2015), 3, 3975–3982, https://doi.org/10.1016/j.ceramint.2014.11.082.
90. L. V. Dihoru, L. N. Smith, R. M. German, Experimental analysis and neural network modelling of the rheological behaviour of powder injection moulding feedstocks formed with bimodal powder mixtures, Powder Metall., 43 (2000), 1, 31–36, https://doi.org/10.1179/pom.2000.43.1.31.
91. H. Oh, T. Im, J. Pyo, J. Lee, C. S. Lee, Study of solid loading of feedstock using trimodal iron powders for extrusion based additive manufacturing, Sci. Rep., 13 (2023), 1, 4819, https://doi.org/10.1038/s41598-023-32095-5.
92. A. Mityukov, V. Govorov, A. Malkin, V. Kulichikhin, Rheology of highly concentrated suspensions with a bimodal size distribution of solid particles for powder injection molding, Polymers, 13 (2021), 16, 2709, https://doi.org/10.3390/polym13162709.
93. B. N. Mukund, B. Hausnerova, T. S. Shivashankar, Development of 17 4PH stainless steel bimodal powder injection molding feedstock with the help of interparticle spacing/lubricating liquid concept, Powder Technol., 283 (2015), 24–31, https://doi.org/10.1016/j.powtec.2015.05.013.
94. J. J. Griebler, A. S. Tappan, S. A. Rogers, A. M. Grillet, J. W. Kopatz, Printability criterion and filler characteristics model for material extrusion additive manufacturing, Addit. Manuf., 99 (2025), 104651, https://doi.org/10.1016/j.addma.2025.104651.
95. K. Rane, L. Di Landro, M. Strano, Processability of SS316L powder binder mixtures for vertical extrusion and deposition on table tests, Powder Technol., 345 (2019), 553–562, https://doi.org/10.1016/j.powtec.2019.01.010.
96. F. M. Barreiros, M. T. Vieira, PIM of non conventional particles, Ceram. Int., 32 (2006), 3, 297–302, https://doi.org/10.1016/j.ceramint.2005.03.006.
97. E. Hnatkova, B. Hausnerova, P. Filip, Evaluation of powder loading and flow properties of Al2O3 ceramic injection molding feedstocks treated with stearic acid, Ceram. Int., 45 (2019), 16, 20084–20090, https://doi.org/10.1016/j.ceramint.2019.06.273.
98. T. M. Abu Lebdeh, O. A. Kalejaiye, Evaluation of binary and ternary models in powder packing density for additive manufacturing applications, Am. J. Eng. Appl. Sci., 14 (2021), 2, 314–322, https://doi.org/10.3844/ajeassp.2021.314.322.
99. T. Honek, B. Hausnerova, P. Saha, Relative viscosity models and their application to capillary flow data of highly filled hard metal carbide powder compounds, Polym. Compos., 26 (2005), 1, 29–36, https://doi.org/10.1002/pc.20067.
100. B. Hausnerova, J. Zidek, An analytical approach to relating powder characteristics and rheological properties of powder injection molding feedstocks, Ceram. Int., 42 (2016), 15, 17045–17052, https://doi.org/10.1016/j.ceramint.2016.07.212.
101. Y. Park, S. J. Park, Particle size dependent viscosity behavior of a suspension using image processing, Powder Technol., 339 (2018), 686–694, https://doi.org/10.1016/j.powtec.2018.08.049.
102. B. Hausnerova, P. Filip, Processability of high metal and ceramic concentration compounds, in: Encyclopedia of Materials: Composites, 1st ed., vol. 2, D. Brabazon (Ed.), Elsevier, 2021, pp. 855–872, https://doi.org/10.1016/B978-0-12-819724-0.00030-6.
103. C. Kukla, I. Duretek, J. Gonzalez Gutierrez, C. Holzer, Rheology of PIM feedstocks, Met. Powder Rep., 72 (2017), 1, 39–44, https://doi.org/10.1016/j.mprp.2016.03.003.
104. J. Gonzalez Gutierrez, M. Spoerk, M. Arbeiter, D. Godec, C. Holzer, Models to predict the viscosity of metal injection molding feedstock materials as function of their formulation, Metals, 6 (2016), 6, 129, https://doi.org/10.3390/met6060129.
105. M. Khakbiz, A. Simchi, R. Bagheri, Analysis of the rheological behavior and stability of 316L stainless steel–TiC powder injection molding feedstock, Mater. Sci. Eng. A, 407 (2005), 1–2, 105–113, https://doi.org/10.1016/j.msea.2005.06.057.
106. P. Suri, S. V. Atre, R. M. German, J. P. de Souza, Effect of mixing on the rheology and particle characteristics of tungsten based powder injection molding feedstock, Mater. Sci. Eng. A, 356 (2003), 1–2, 337–344, https://doi.org/10.1016/S0921-5093(03)00146-1.

107. R. Zauner, C. Binet, D. F. Heaney, J. Piemme, Variability of feedstock viscosity and its correlation with dimensional variability of green powder injection moulded components, Powder Metall., 47 (2004), 2, 150–155, https://doi.org/10.1179/003258904225015473.
108. D. Pettas, G. Karapetsas, Y. Dimakopoulos, J. Tsamopoulos, On the origin of extrusion instabilities: Linear stability analysis of the viscoelastic die swell, J. Non Newton. Fluid Mech., 224 (2015), 61–77, https://doi.org/10.1016/j.jnnfm.2015.07.011.
109. P. Filip, B. Hausnerova, C. Barretta, Master flow curves as a tool to modelling ceramic injection molding, Ceram. Int., 45 (2019), 6, 7468–7471, https://doi.org/10.1016/j.ceramint.2019.01.038.
110. P. Filip, B. Hausnerova, E. Hnatkova, Continuous rheological description of highly filled polymer melts for material extrusion, Appl. Mater. Today, 20 (2020), 100754, https://doi.org/10.1016/j.apmt.2020.100754.
111. M. Strano, K. Rane, F. Briatico Vangosa, L. Di Landro, Extrusion of metal powder polymer mixtures: Melt rheology and process stability, J. Mater. Process. Technol., 273 (2019), 116250, https://doi.org/10.1016/j.jmatprotec.2019.116250.
112. A. V. Shenoy, Rheology of filled polymer systems, Kluwer Academic Publishers, Dordrecht, 1999.
113. J. A. Naranjo, C. Berges, R. Campana, G. Herranz, Rheological and mechanical assessment for formulating hybrid feedstock to be used in MIM & FFF, Results Eng., 19 (2023), 101258, https://doi.org/10.1016/j.rineng.2023.101258.
114. M. M. Amin, N. Muhamad, A. B. Sulong, A. Basir, N. A. M. A. Tamizi, Flowability and moldability of zirconia micro part via micro powder injection molding, J. Kejuruteraan, 36 (2024), 5, 2107–2114, https://doi.org/10.17576/jkukm-2024-36(5)-27.
115. M. A. Ahmad, N. Johari, M. J. Sulaiman, R. Ibrahim, M. A. Omar, Rheological evaluation of titanium alloy metal injection molding (MIM) feedstock, Saudi J. Eng. Technol., (2021), https://doi.org/10.36348/sjet.2021.v06i11.003.
116. J. Wang, Q. Shi, C. Wu, J. Xi, Rheological characteristics of injection molded titanium alloys powder, Trans. Nonferrous Met. Soc. China, 23 (2013), 9, 2605–2610, https://doi.org/10.1016/S1003-6326(13)62774-0.
117. J. M. Contreras, A. Jiménez Morales, J. M. Torralba, Experimental and theoretical methods for optimal solids loading calculation in MIM feedstocks fabricated from powders with different particle characteristics, Powder Metall., 53 (2010), 1, 34–40, https://doi.org/10.1179/003258909X12450768327225.
118. T. Honek, B. Hausnerova, P. Saha, Temperature dependent flow properties of powder injection moulding compounds, Appl. Rheol., 12 (2002), 72–80, https://doi.org/10.3933/ApplRheol-12-72.
119. C. Dimitri, S. Mohamed, B. Thierry, G. Jean Claude, Influence of particle size distribution and temperature on the rheological properties of highly concentrated Inconel feedstock alloy 718, Powder Technol., 322 (2017), 273–289, https://doi.org/10.1016/j.powtec.2017.08.049.
120. B. Hausnerova, T. Sedlacek, R. Slezak, P. Saha, Pressure dependent viscosity of powder injection moulding compounds, Rheol. Acta, 45 (2006), 3, 290–296, https://doi.org/10.1007/s00397-005-0036-4.
121. C. D. Greene, D. F. Heaney, The PVT effect on the final sintered dimensions of powder injection molded components, Mater. Des., 28 (2007), 1, 95–100, https://doi.org/10.1016/j.matdes.2005.05.023.
122. H. Persson, B. Hausnerova, L. Nyborg, M. Rigdahl, Rheological and thermal properties of a model system for PIM, Int. Polym. Process., 24 (2009), 2, 206–212, https://doi.org/10.3139/217.2243.
123. B. Hausnerova, L. Cucova, A. Sorrentino, Effect of carbide powder characteristics on the PVT behavior of powder injection molding compounds, Powder Technol., 237 (2013), 627–633, https://doi.org/10.1016/j.powtec.2013.01.067.
124. V. Onbattuvelli, K. R. Enneti, S. B. Sohn, T. McCabe, S. J. Park, S. Atre, Micro powder injection moulding of barium titanate, PIM Int., 5 (2011), 59–65.
125. K. H. Kate, V. P. Onbattuvelli, R. K. Enneti, S. W. Lee, S. J. Park, S. V. Atre, Measurements of powder–polymer mixture properties and their use in powder injection molding simulations for aluminum nitride, JOM, 64 (2012), 9, 1048–1058, https://doi.org/10.1007/s11837-012-0404-3.

126. J. Lenz, R. K. Enneti, V. Onbattuvelli, K. Kate, R. Martin, S. Atre, Powder injection molding of ceramic engine components for transportation, JOM, 64 (2012), 3, 388–392, https://doi.org/10.1007/s11837-012-0264-x.
127. M. Lee, J. H. Yu, J. H. Kim, S. J. Park, I. D. Jung, Process/design optimization for powder injection molding of turbocharger vane by rheological & computational analysis, Met. Powder Rep., (2020), https://doi.org/10.1016/j.mprp.2020.02.002.
128. N. Fu, N. H. Loh, S. B. Tor, B. Y. Tay, Y. Murakoshi, R. Maeda, Analysis of demolding in micro metal injection molding, Microsyst. Technol., 12 (2006), 6, 554–564, https://doi.org/10.1007/s00542-005-0071-1.
129. Z. Hashin, Analysis of composite materials — A survey, J. Appl. Mech., 50 (1983), 3, 481–505, https://doi.org/10.1115/1.3167081.
130. R. A. Schapery, Thermal expansion coefficients of composite materials based on energy principles, J. Compos. Mater., 2 (1968), 3, 380–404, https://doi.org/10.1177/002199836800200308.
131. J. Wang, P. Xie, W. Yang, Y. Ding, Online pressure–volume–temperature measurements of polypropylene using a testing mold to simulate the injection molding process, J. Appl. Polym. Sci., 118 (2010), 1, 200–208, https://doi.org/10.1002/app.32070.
132. N. M. Rudolph, T. A. Osswald, G. W. Ehrenstein, Influence of pressure on volume, temperature and crystallization of thermoplastics during polymer processing, Int. Polym. Process., 26 (2011), 3, 239–248, https://doi.org/10.3139/217.2417.
133. K. Rienesl, Squeeze flow rheometry of carbon fiber SMCs: Design, analysis and simulation, Master's thesis, Universität Linz, 2023.
134. A. N. Muranov, A. B. Semenov, A. A. Kutsbakh, B. I. Semenov, Specific volume and features of compaction in molding of powder–polymer mixtures with wax–polypropylene binder, Polym. Sci. Ser. D, 13 (2020), 2, 228–234, https://doi.org/10.1134/S1995421220020173.
135. A. Das, E. L. Gilmer, S. Biria, M. J. Bortner, Importance of polymer rheology on material extrusion additive manufacturing: Correlating process physics to print properties, ACS Appl. Polym. Mater., 3 (2021), 3, 1218–1249, https://doi.org/10.1021/acsapm.0c01228.
136. B. K. Brettmann, J. Kalman, J. M. McCollum, L. M. J. Moore, A. M. Savage, M. S. McClain, Challenges and opportunities in manufacturing highly filled polymers, Adv. Manuf., 2 (2025), 1, 34, https://doi.org/10.1038/s44334-025-00046-9.
137. K. Rane, T. Barriere, M. Strano, Role of elongational viscosity of feedstock in extrusion based additive manufacturing of powder binder mixtures, Int. J. Adv. Manuf. Technol., 107 (2020), 11–12, 4389–4402, https://doi.org/10.1007/s00170-020-05323-9.
138. T. Sedlacek, R. Cermak, B. Hausnerova, M. Zatloukal, A. Boldizar, P. Saha, On PVT and rheological measurements of polymer melts, Int. Polym. Process., 20 (2005), 3, 286–295, https://doi.org/10.3139/217.1890.
139. B. Hausnerova, T. Sedlacek, P. Vltavska, Pressure affected flow properties of powder injection moulding compounds, Powder Technol., 194 (2009), 3, 192–196, https://doi.org/10.1016/j.powtec.2009.04.007.
140. B. Hausnerova, T. Sedlacek, P. Filip, P. Saha, The effect of powder characteristics on pressure sensitivity of powder injection moulding compounds, Powder Technol., 206 (2011), 3, 209–213, https://doi.org/10.1016/j.powtec.2010.08.065.
141. N. Y. Zhao, J. F. Liu, M. Y. Su, Z. B. Xu, Measurement techniques in injection molding: A comprehensive review, Measurement, 226 (2024), 114163, https://doi.org/10.1016/j.measurement.2024.114163.
142. S. Shivashankar, R. K. Enneti, S. J. Park, R. M. German, S. V. Atre, The effects of material attributes on powder–binder separation phenomena in powder injection molding, Powder Technol., 243 (2013), 79–84, https://doi.org/10.1016/j.powtec.2013.03.037.
143. M. Jenni, R. Zauner, J. Stampfl, Powder injection moulding — Quality & simulation: Measurement methods for powder binder separation in PIM components, in: Proc. Euro PM 2009 — European Powder Metallurgy Congress & Exhibition, European Powder Metallurgy Association, 2009, pp. 141–146.
144. S. Yang, R. Zhang, X. Qu, X ray analysis of powder binder separation during SiC injection process in L shaped mould, J. Eur. Ceram. Soc., 35 (2015), 1, 61–67, https://doi.org/10.1016/j.jeurceramsoc.2014.08.022.

145. J. L. Colón Quintana, T. Heckner, A. Chrupala, J. Pollock, S. Goris, T. Osswald, Experimental study of particle migration in polymer processing, Polym. Compos., 40 (2019), 6, 2165–2177, https://doi.org/10.1002/pc.25018.
146. L. Urtekin, F. Bozkurt, M. Çanli, Analysis of biomedical titanium implant green parts by X ray tomography, J. Mater. Res. Technol., 14 (2021), 277–286, https://doi.org/10.1016/j.jmrt.2021.06.083.
147. O. Weber, A. Rack, C. Redenbach, M. Schulz, O. Wirjadi, Micropowder injection molding: Investigation of powder-binder separation using synchrotron-based microtomography and 3D image analysis, J. Mater. Sci., 46 (2011), 10, 3568–3573, https://doi.org/10.1007/s10853-011-5270-9.
148. B. Hausnerova, D. Sanetrnik, P. Ponizil, Surface structure analysis of injection molded highly filled polymer melts, Polym. Compos., 34 (2013), 9, 1553–1558, https://doi.org/10.1002/pc.22572.
149. D. Sanetrnik, B. Hausnerova, P. Ponizil, M. Novak, K. Monkova, Flow-induced defects during metal injection molding: Role of powder morphology, Phys. Fluids, 36 (2024), 8, https://doi.org/10.1063/5.0219410.
150. D. Sanetrnik, B. Hausnerova, M. Novak, B. N. Mukund, Effect of particle size and shape on wall slip of highly filled powder feedstocks for material extrusion and powder injection molding, 3D Print. Addit. Manuf., 10 (2023), 2, 236–244, https://doi.org/10.1089/3dp.2021.0157.
151. D. Sanetrnik, B. Hausnerova, V. Pata, Online rheometry investigation of flow/slip behavior of powder injection molding feedstocks, Polymers, 11 (2019), 3, 432, https://doi.org/10.3390/polym11030432.
152. S. P. Meeker, R. T. Bonnecaze, M. Cloitre, Slip and flow in pastes of soft particles: Direct observation and rheology, J. Rheol., 48 (2004), 1295–1320, https://doi.org/10.1122/1.1795171.
153. S. Aktas, D. M. Kalyon, B. M. Marin-Santibanez, J. Perez-Gonzalez, Shear viscosity and wall slip behavior of a viscoplastic hydrogel, J. Rheol., 58 (2014), 513–535, https://doi.org/10.1122/1.4866295.
154. Y. Chen, D. M. Kalyon, E. Bayramli, Effects of surface roughness and the chemical structure of materials of construction on wall slip behavior of linear low density polyethylene in capillary flow, J. Appl. Polym. Sci., 50 (1993), 1169–1177, https://doi.org/10.1002/app.1993.070500707.
155. M. Jeong, Y. Kim, W. Zhou, W. Q. Tao, M. Y. Ha, Effects of surface wettability, roughness and moving wall velocity on the Couette flow in nano-channel using multi-scale hybrid method, Comput. Fluids, 147 (2017), 1–11, https://doi.org/10.1016/j.compfluid.2017.01.021.
156. H. A. Barnes, A review of the slip (wall depletion) of polymer solutions, emulsions and particle suspensions in viscometers: Its cause, character, and cure, J. Non-Newton. Fluid Mech., 56 (1995), 221–251, https://doi.org/10.1016/0377-0257(94)01282-M.
157. M. Kubisova, V. Pata, D. Merinska, A. Skrobak, M. Marcanik, Solving the issue of discriminant roughness of heterogeneous surfaces using elements of artificial intelligence, Materials, 14 (2021), 2620, https://doi.org/10.3390/ma14102620.
158. H. Vrbova, M. Kubisova, D. Merinska, M. Novak, V. Pata, J. Knedlova, M. Sedlacik, O. Suba, The implementation of neural networks for polymer mold surface evaluation, Micromachines, 15 (2024), 1, 102, https://doi.org/10.3390/mi15010102.
159. D. Sanetrnik, B. Hausnerova, P. Filip, E. Hnatkova, Influence of capillary die geometry on wall slip of highly filled powder injection molding compounds, Powder Technol., 325 (2018), 615–619, https://doi.org/10.1016/j.powtec.2017.11.041.
160. A. G. Hasib, S. Niauzorau, W. Xu, S. Niverty, N. Kublik, J. Williams, N. Chawla, K. Song, B. Azeredo, Rheology scaling of spherical metal powders dispersed in thermoplastics and its correlation to the extrudability of filaments for 3D printing, Addit. Manuf., 41 (2021), 101967, https://doi.org/10.1016/j.addma.2021.101967.
161. S. Haavisto, M. Cardona, J. Salmela, R. L. Powell, M. McCarthy, M. Kataja, A. I. Koponen, Experimental investigation of the flow dynamics and rheology of complex fluids in pipe flow by hybrid multi-scale velocimetry, Exp. Fluids, 58 (2017), 11, 158, https://doi.org/10.1007/s00348-017-2440-9.
162. A. Mannschatz, S. Höhn, T. Moritz, Powder-binder separation in injection moulded green parts, J. Eur. Ceram. Soc., 30 (2010), 14, 2827–2832, https://doi.org/10.1016/j.jeurceramsoc.2010.02.020.

163. M. Schwaiger, Experimental and numerical investigation of special flow phenomena in powder injection molding, Master's thesis, 2019.
164. K. J. LeBlanc, S. R. Niemi, A. I. Bennett, K. L. Harris, K. D. Schulze, W. G. Sawyer, C. Taylor, T. E. Angelini, Stability of high speed 3D printing in liquid-like solids, ACS Biomater. Sci. Eng., 2 (2016), 10, 1796–1799, https://doi.org/10.1021/acsbiomaterials.6b00184.
165. N. T. Saidy, T. Shabab, O. Bas, D. M. Rojas-González, M. Menne, T. Henry, D. W. Hutmacher, P. Mela, E. M. De-Juan-Pardo, Melt electrowriting of complex 3D anatomically relevant scaffolds, Front. Bioeng. Biotechnol., 8 (2020), 793, https://doi.org/10.3389/fbioe.2020.00793.
166. A. Maciel, V. Salas, J. F. A. Soltero, J. Guzmán, O. Manero, On the wall slip of polymer blends, J. Polym. Sci. B Polym. Phys., 40 (2002), 4, 303–316, https://doi.org/10.1002/polb.10093.
167. S. S. Vadodaria, A. J. Onyianta, D. Sun, High-shear rate rheometry of micro-nanofibrillated cellulose (CMF/CNF) suspensions using rotational rheometer, Cellulose, 25 (2018), 10, 5535–5552, https://doi.org/10.1007/s10570-018-1963-4.
168. G. Zitzenbacher, T. Bayer, Z. Huang, Influence of tool surface on wall sliding of polymer melts, Int. J. Mater. Prod. Technol., 52 (2015), 17–36, https://doi.org/10.1504/IJMPT.2016.073617.
169. M. P. Bryan, S. L. Rough, D. I. Wilson, Measurement of the wall slip behaviour of a solid granular soap in ram extrusion, Powder Technol., 323 (2018), 76–85, https://doi.org/10.1016/j.powtec.2017.09.053.
170. S. A. O. Nair, H. Alghamdi, A. Arora, I. Mehdipour, G. Sant, N. Neithalath, Linking fresh paste microstructure, rheology and extrusion characteristics of cementitious binders for 3D printing, J. Am. Ceram. Soc., 102 (2019), 7, 3951–3964, https://doi.org/10.1111/jace.16305.
171. H. Alghamdi, S. A. O. Nair, N. Neithalath, Insights into material design, extrusion rheology, and properties of 3D-printable alkali-activated fly ash-based binders, Mater. Des., 167 (2019), 107634, https://doi.org/10.1016/j.matdes.2019.107634.
172. A. Delime, M. Moan, Lateral migrations of solid spheres in tube flow, Rheol. Acta, 30 (1991), 2, 131–139, https://doi.org/10.1007/BF01134602.
173. Y. C. Lam, X. Chen, K. W. Tan, J. C. Chai, S. C. M. Yu, Numerical investigation of particle migration in Poiseuille flow of composite system, Compos. Sci. Technol., 64 (2004), 7–8, 1001–1010, https://doi.org/10.1016/j.compscitech.2003.08.005.
174. C. Kukla, I. Duretek, C. Holzer, Controlled shear stress method to measure yield stress of highly filled polymer melts, AIP Conf. Proc., 1779 (2016), 070006, https://doi.org/10.1063/1.4965538.
175. A. J. Poslinski, M. E. Ryan, R. K. Gupta, S. G. Seshadri, F. J. Frechette, Rheological behavior of filled polymeric systems. I. Yield stress and shear-thinning effects, J. Rheol., 32 (1988), 703–735, https://doi.org/10.1122/1.549987.
176. W. J. Tseng, K.-H. Teng, Effect of surfactant adsorption on aggregate structure and yield strength of zirconia-wax suspensions, J. Mater. Sci., 36 (2001), 173–178, https://doi.org/10.1023/A:1004805523977.
177. D. M. Liu, W. J. Tseng, Yield behavior of zirconia-wax suspensions, Mater. Sci. Eng. A, 254 (1998), 136–146, https://doi.org/10.1016/S0921-5093(98)00699-6.
178. R. Eickhoff, S. Antusch, S. Baumgärtner, D. Nötzel, T. Hanemann, Feedstock development for material extrusion-based printing of Ti6Al4V parts, Materials, 15 (2022), 18, 6442, https://doi.org/10.3390/ma15186442.